Very detailed seismic pattern and migration inferred from the April 2010 Pietralunga (northern Italian Apennines) micro-earthquake sequence

Simone Marzorati[a,*], Marco Massa[b], Marco Cattaneo[a], Giancarlo Monachesi[a], Massimo Frapiccini[a]

[a] Istituto Nazionale di Geofisica e Vulcanologia, Centro Nazionale Terremoti, Via di Colle Ameno 5, 60129, Ancona (AN), Italy

[b] Istituto Nazionale di Geofisica e Vulcanologia, Sezione di Milano, via Bassini 15, 20133, Milano (MI), Italy

***Corresponding author: Simone Marzorati**

Centro Nazionale Terremoti

Istituto Nazionale di Geofisica e Vulcanologia (INGV)

Via di Colle Ameno 5

60126 Ancona (AN), Italy

Tel: +39-071-8067720

E-mail: simone.marzorati@ingv.it

Abstract

We propose a very detailed picture of seismicity that occurred in the proximity of the Alto Tiberina Low Angle Normal Fault (ATF, northern Italian Apennines), by presenting the pattern and evolution of a seismic sequence on the hanging wall of the ATF in the first months of 2010 that was characterized by about 1000 events with ML ranging from -0.7 to 3.8.

To capture the rupture kinematics of the investigated area, a cross-correlation technique was initially applied to calculate very accurate time shifts among the events of the sequence, and then to relocate them. The whole sequence was relocated with the double-difference method, which includes both absolute travel-time measurements and cross-correlation differential travel-times. The new locations confirm that the seismic activity was mainly arranged along a NW-SE-oriented structure that, ranged in depth from 4 km to 6 km, with dipping towards NE at an angle of ca. 65°. In comparison with geological data, the position of the seismic sequence is compatible with the Evaporite Triassic layer. The main nodal planes are consistent with the spatial evolution of the aftershocks and with the tensional state of stress in the area.

An analysis of waveform similarity was performed at a reference station by merging the capability of the cross-correlation technique and the bridging algorithm. The detected mutiplets allow us to emphasize the anisotropic spatial and temporal migration of the seismicity that occurred along a 307°N strike direction with an averaged propagation velocity of ca. 0.4 km/day. We explain the highlighted anisotropic behavior of the migration with the hypothesized presence of overpressured fluids and with physical properties of Triassic Evaporites. This suggests the importance of such very detailed relocation of weak and micro seismicity for improvement of our knowledge of fault system geometry and its evolution.

Key words: cross-correlation; multiplets; double difference; migration; pattern; Alto Tiberina Fault

1. Introduction

The accurate location of microseismicity occurrences makes it possible to discover fault architecture and to provide very detailed pictures of fault systems (Chiaraluce et al., 2011). However, preliminary earthquake locations after seismic sequences and swarms depict a large-scale (kilometer) spatial description of fault zones. The relatively high magnitude of completeness characterizes earthquake catalogs of seismic sequences and prevents precise descriptions of fault systems (Wiemer and Wyss, 2000; Valoroso et al., 2013).

Over last decade, the performances and dynamics of three-component seismic instruments and the growth of seismic networks has provided the scientific community with the opportunity to analyze earthquake data obtained with improved magnitude detection thresholds and improved network resolution. Furthermore, several methods have been developed to more precisely and accurately define earthquake locations (Got et al., 1994, Waldhauser and Ellsworth, 2000). These recent improvements have allowed investigations into the detailed geometry of active faults and the observation of seismic migration through the spatio-temporal evolution of the seismicity (Pacchiani and Lyon-Caen, 2009; Chiaraluce et al., 2011; Valoroso et al., 2013).

As well as earthquake relocation, analysis of earthquake similarity can provide other information about the rheological properties, kinematic behaviour, and spatio-temporal evolution of a fault system (Valoroso et al., 2013). Clusters of similar events have been investigated using several techniques: cross-spectral techniques (Got et. al., 1994; Scherbaum and Wendler, 1986), pattern recognition (Joswig, 1995), fractal approaches (Smalley et al., 1987), syntactic pattern recognition schemes (Zhinzhin et al., 1992; 1994), non-linear correlation techniques (Schulte-Theis and Joswig, 1993), dendogram analysis (Schulte-Theis, 1995), and cross-correlation techniques (e.g., Augliera et al., 1995; Cattaneo et al., 1997, 1999; Ferretti et al., 2005; Massa et al., 2006a, 2006b).

In the present study, new seismological insights and more detailed features were investigated relating to the microseismicity in the northern Italian Apennines associated with the spatio-temporal evolution of the April 2010, M_L 3.8, seismic sequence (hereinafter referred to as the Pietralunga sequence). The April 15, 2010, mainshock triggered a relevant number of aftershocks, which extended for about one month, which as provided a dataset composed of about 1000 weak

earthquakes (smallest M_L below 0). These occurred at shallow crustal levels between 4 km and 6 km in depth, and they were recorded by a dense seismic network that is equipped with high dynamic, high performance three-component digital instruments. The seismic network covers the area over the Alto Tiberina Fault (ATF), a low angle normal fault (LANF) that acts as a basal seismic detachment and accommodates extensional deformation together with a complex normal fault system that is located in its hanging wall (Chiaraluce et al., 2007). The ATF is a topic of debate relating to the possibility that moderate-to-large earthquakes nucleate on LANFs or that creeping is the fault style (Chiaraluce et al., 2007, and references therein). In the tectonic setting of the Italian Apennines, seismicity migration episodes along the strike of a fault system or along a preferred direction can be observed during seismic sequences related to moderate earthquakes: e.g., the M_w 5.9 1997 Colfiorito earthquake (Cataldi et al., 2008), and the M_w 6.1 2009 L'Aquila earthquake (Chiaraluce et al., 2011). These migrations are often related to the presence of overpressurized fluids and to diffusion processes (Noir et al., 1997; Miller et al., 2004; Antonioli et al., 2005). The monitoring and detailed reconstruction of seismicity patterns and the spatio-temporal evolution in the extensional tectonic Italian Apennine context is important to understand the preparatory phases of the main earthquakes (Chiaraluce et al., 2011).

In the present study, we have used precise manual P-phase and S-phase catalogs to apply the double-difference technique (Waldhauser, 2001; Waldhauser and Ellsworth, 2000) to relocate events. This is combined with the bridging technique, which has been proposed by many authors (e.g., Aster and Scott, 1993; Cattaneo et al. 1997, 1999; Deichmann and Garcia-Fernandez, 1992; Ferretti et al., 2005; Massa et al., 2006a) to gather the Pietralunga sequence into families of similar events.

After a brief description of the tectonic setting and the seismicity of the area, the relocation and seismicity pattern of the Pietralunga sequence is described through consideration of a restricted dataset that is composed of multiplets that were determined by adopting a cross-correlation coefficient threshold of 0.75 at a reference station. Moreover, the seismicity migration is described based on only the relocated events that are included in the multiplets obtained with a threshold of 0.90, to enhance the coherence of the related events.

The accurate relative location of these events allows the reconstruction of the precise geometry of the sequence, through locating its seismicity in the context of the complex normal fault system of the ATF hanging wall. We calculate focal mechanisms of the largest events (M_L ≥2) to understand the general kinematics of the structure highlighted by the sequence. Also, the relative locations allow us to hypothesize that this seismicity is related to the Triassic Evaporite geological layer. We analyse the style of the seismicity migration by mapping the spatio-temporal evolution of clusters of similar events. Finally, we note the detailed behavior of the migration that we relate to the rheological properties of the Triassic Evaporites and with to the pressurized fluids in different sections of the geological layer, as observed in exploration studies (Chiodini and Cioni, 1989; Trippetta et al., 2013).

2. Tectonic setting and seismicity

The northern Apennines are characterized by a NE-verging thrust-fold belt that has arisen as a consequence of the collision between the European continental margin and the Adriatic lithosphere (Alvarez, 1972; Reutter et al., 1980). During the eastward migration in Early Miocene of the two NW-SE belts towards Tuscany, a compressive and an extensional front coexisted (e.g., Barchi et al., 2006). The earlier compressive phase was followed by an extensional phase (which is ongoing) that involves the Umbria region (Ambrosetti et al., 1978). In the western part of the Umbria-Marche Apennines, the ATF, whic is part of a system of east-dipping LANFs (Boncio et al., 2000; Jolivet et al., 1998), and the associated high-angle antithetic structures, accommodate the extension zone within the brittle upper crust. The ATF bounds the western side of the upper Tiber Quaternary basin, and it is about 70 km long, dips from 15° to 20° ENE (Chiaraluce et al, 2007, Mirabella et al. 2011), and is clearly evident in the CROP03-NVR seismic reflection profiles (Barchi et al. 1998a, 1998b; Pialli et al., 1998). The ATF has been reconstructed by surface geological surveys and subsurface geological and geophysical data (Mirabella et al. 2011). In the last decade, several studies of the ATF and its surroundings hare been carried out (Chiaraluce et al., 2007; Collettini and Barchi, 2002; Piccinini et al., 2003) with the aim of investigating the associated seismicity rate.

The micro-seismicity associated with the ATF is probably triggered by frictional instabilities that are created by fluid overpressure, while the most of the extension along the fault is accommodated by aseismic slip and creep (Chiaraluce et al., 2007; Collettini and Barchi, 2002). An open issue relates to the possible occurrence of moderate-to-large earthquakes generated by LANFs (Chiaraluce et al., 2007, and references therein; Wernicke, 1995), and, as a consequence, therelevance of LANFs in terms of seismic hazard.

Weak to moderate earthquakes (DBMI11, Locati et al., 2011) occurred in the area in 1693 (Alta Valtiberina, Io 6-7, Mw 4.9, from macroseismic data), 1897 (Appennino Umbro-Marchigiano, Io 7, Mw 5.13, from macroseismic data), 1917 (Valtiberina, Io 9-10, Mw 5.89, from macroseismic data) and 1948 (Valtiberina, Io 7, Mw 5.05 from macroseismic data). The strongest earthquakes over the last 30 years occurred in 1984 (the Gubbio-Valfabbrica earthquake, Io 7, Mw 5.1), 1997 (Umbria-Marche Apennines, Mw 6.0, 5.7 and 5.6) and 1998 (Umbria-Marche Apennines, Mw 5.1). These events were characterized by seismic sequences with shock-aftershock behavior (Chiaraluce et al., 2004). The focal mechanisms of these instrumental events showed extensional normal faults that were SW-dipping (Chiaraluce et al., 2007); it is worth mentioning that the dip of these mechanisms is opposite with respect to the observed ATF dip (15° towards NE). The hypocenters of these mainshocks and the related sequences were distributed on the antithetic planes that lie on the hanging wall of the ATF.

By analysing a dataset of weak events collected during a 2000-2001 seismic survey (Piccinini et al., 2003), Chiaraluce et al. (2007) relocated about 2000 earthquakes with M_L <3.1, to fix the geometry and the main features of the ATF. From the micro-seismicity relocation, we can highlight not only the main plane of the ATF, but also the presence of two second-order faults that are located in the hanging wall of the ATF: a gently eastward-dipping synthetic fault, and a high-angle antithetic west-dipping fault, in agreement with the faults mapped during the 1984 Gubbio-Valfabbrica earthquake.

3. Seismic data

The earthquakes analyzed in the present study were recorded by the seismic networks of central-eastern Italy (ReSIICO; Monachesi et al., 2013) that are managed by the Italian National Institute for Geophysics and Vulcanology (INGV) in cooperation with the Regional Multi-Risk Department of Civil Protection of the Marche Region (Fig. 1). The ResiICO includes data recorded in real time by the stations of the National Seismic Network (NSN; Amato and Mele, 2008; Delladio, 2011) and the Alto Tiberina Seismic Network (ATSN). The ATSN is a dense network that was installed in the framework of The Alto tiBerina near fault ObservatOry (TABOO; taboo.rm.ingv.it) infrastructure and it has been devoted to the monitoring of the ATF (Chiaraluce et al., 2007; Collettini and Chiaraluce, 2013), which is one of the rare examples worldwide of a true LANF.

The ATSN is a dense seismic network that has been operating at full capacity since August 2009. Its transmission is based on WiFi connections that are linked to the 155 Mb Marche-Way radio network, and it sends a continuous data stream to the acquisition center of INGV Ancona (Monachesi and Cattaneo, 2010). The ATSN stations used in the present study are equipped with 24 bit INGV-made GAIA2 acquisition systems (Salvaterra et al., 2008) that are coupled to Nanometrics Trillium 40s or Lennartz 5s velocimetric sensors.

The NSN stations are equipped with Nanometrics Trillium 40s, 120s or 240s, or Lennartz 3Dlite1s or 3D-5s velocimetric sensors and Kinemetrics FBA Episensor accelerometers; the acquisition systems are INGV-made GAIA2 and Nanometrics Taurus or Trident.

The continuous signals are recorded in real time at 100 sps and then stored at the INGV acquisition center in Ancona. The seismic eventsare detected by the automatic Earthworm trigger systems (USGS et al., 2010) and are manually picked by an expert operator that assigns P and S weights to indicate the reliability of each singlephase reading. During the routine earthquake location, performed using Hypoellipse code (Lahr, 1979), a one-dimensional velocity model is used that was developed at a regional scale by De Luca et al. (2009).

During April 2010, 1283 events were localized, with M_L ranging from -0.7 to 3.8, and wich depicted an activated area over about 5 km in a NW-SE direction (Fig. 2, red circles,the Pietralunga sequence). The yellow star in Figures 1 and 2 indicates the epicenter of the April 15, 2010 (01:47 UTM), M_L 3.8 event, which was the largest recorded during the Pietralunga sequence. In particular,

15654 P-phases and 15267 S-phases were collected. Using a scale from 0 to 4, the weights for P-phases were set to 0 (i.e., high quality; Gaussian error, 0.025 s) and 1 (good quality; Gaussian error, 0.050) for 47% and 25% of the total readings, respectively. For the S-phases, the percentages for weights 0 and 1 were 45% and 30%, respectively. The share of weights of 0 increases to 52% (P) and 50% (S) if only the closest 16 stations are considered (Fig. 1, red). This earthquake dataset has a magnitude of completeness (M_C) of 0.38. The minimum number of stations used to localize the events was three, although this represents an extreme; indeed, the event with the lowest magnitude (M_L -0.7) was localized with 4 stations, the average number of stations used to localize the events was 13, and 70% of the events were localized between a minimum of 6 and a maximum of 20 stations.

Fig. 2 shows that for the period from August 2009 to April 9, 2010, the background seismicity of the area (Fig. 2, yellow circles) did not involve the Pietralunga sequence sector. After a sudden increase in the occurrence of events from April 10 to April 30 , 2010 (Fig. 2, red circles), in the period from May 2010 to the end of January 2012 (Fig. 2, blue circles), the seismicity surrounded the area of the Pietralunga sequence.

Fig. 3 shows the increase in the seismicity rates in the area. From August 2009 to April 9, 2010, the number of events per day did not exceed 6 events, with an average of 0.2 events per day (Fig. 4, left panel). During the Pietralunga sequence (Fig. 4, central panel), the number of events per day reached a maximum of 254 events, on April 15, 2010. From April 15 to April 18, 2010, there were more than 100 events per day. In the following days, this rate dwindled down to 50, but then increased again to 90 on April 26, 2010. Between May 2010 and January 2012, the number of events per day ranged from 0 to 19 (Fig. 4, right panel), with an average rate of 1.4 events per day.

Fig. 5 shows the magnitude trends during the Pietralunga sequence: more than 80% of the events recorded had M_L between -0.7 and 1.0, and only 30 events exceeding M_L 2.

4. Relative locations and pattern

To investigate the seismicity pattern of Pietralunga sequence, we used the micro seismicity recorded in April 2010 from all of the available seismic stations of the INGV that were installed in this area. To achieve this, the double-difference relocation algorithm was applied, as implemented in the HypoDD code (Waldhauser, 2001; Waldhauser and Ellsworth, 2000).The HypoDD code works by minimizing the residuals between observed and theoretical travel-time differences (or double-differences) for pairs of earthquakes at each station, linking together all of the observed event-station pairs. The double-difference equation that defined the residual is:

$$dr^{ij}_k = (t^i_k - t^j_k)^{obs} - (t^i_k - t^j_k)^{cal} \quad (1),$$

where dr^{ij}_k is the residual between the observed and calculated differential travel-times between two events, the term $(t^i_k - t^j_k)^{obs}$ is the observed travel-time difference between events *i* and *j* recorded at *k* station, and the term $(t^i_k - t^j_k)^{cal}$ is the calculated travel-time difference between these same events. The least-squares solution was found by iteratively adjusting the vector difference between the hypocentral pairs.

From the whole dataset, we selected 976 events that were grouped into 5 multiplets, as detected at the PIEI reference station (Fig. 6a), using a cross correlation threshold of 0.75 (for further details of the method, see Appendix A). This was merely to extract from the seismicity of the area the events that are members of the sequence cluster and that have such a degree of similarity. Moreover, 5 earthquakes with ML ≥ 2 were localized in the cluster of the Pietralunga sequence, but were not included in any of the multiplets by the automatic analyses; these were added manually. Fig. 6a shows the selected events (blue circles). In order to relocate the events, the arrival times that were obtained in the manual pick of the P-phases and S-phases (see above) for the stations indicated by the red triangles in Fig. 1 were combined with the differential travel-times obtained by the cross-correlation analyses. This was performed considering windows 1.5 s long, starting from the P-phases and S-phase onsets. To assign the relative weights to these differential travel-times, we used the square of the cross-correlation value. The double-difference relocation algorithm detected two clusters of events. The first had the pattern shown in Fig.6b (red circles) after the

relocation procedure. The relocated epicenters consisted of a narrow alignment of seismicity that developed along the main NW-SE Apennine direction (azimuth of about 307 °N). The transverse profile of the seismicity highlights the NE deepening of the narrow cluster of events (Fig. 7, red circles), with an angle of about 65° with respect to the ground surface. The relocation procedure allowed us to draw up the simple but accurate geometry: about 5 km long and 2.5 km wide. The structure revealed by the relocated seismicity is synthetic with respect to the ATF hanging wall, which in this area lies at a depth of between 6 km and 7 km. It is worth mentioning that the relocated Pietralunga sequence is coherent with the F1 synthetic structure reported in Chiaraluce et al. (2007). The second cluster (Fig. 6b and Fig.7, magenta circles) includes a parallel alignment that was located to the NE (Fig. 6b) and was detached from the first cluster (Fig. 7).

The pattern of the Pietralunga sequence was investigated by following a relocation scheme using HypoDD. All of the events of the sequence were relocated to provide the whole dataset of differential travel-times obtained from the analyzed cross-correlation and the absolute arrival times. The aim was to obtain a unique cluster that showed the overall geometry of the structure. The stability of the relocation process and the resulting shape of the structure revealed were checked considering the azimuthal gap, the number of phases, and the different cross-correlation thresholds. The azimuthal gap of the relocation ranged between 61° and 150° for the 90% of the data; moreover, 97.75% of the data showed a gap <180° (Fig. 8a). At least six phases (three P-phases, three S-phases) were used to relocate the 981 events selected, and 12 phases were used to relocate 90% of the data; 50% of the events were relocated with at least 22 phases (Fig. 8b). Fig. 8c ,d presents the results of the sensitivity analysis. With the aim of quantifying the uncertainties in the model outputs on a quality level (i.e., the relocated hypocenters) with respect to different inputs, the events selected on the basis of the squared cross-correlation threshold were evaluated. Although a few events were lost in moving towards the higher cross-correlation, in general, the shape of the main cluster did not change, neither in terms of its position on the map, nor in terms of its depth, thus confirming the reliability of the data presented.

5. Seismicity migration

Starting from the 981 relocated events that allowed the highlighting of the seismicity pattern of the Pietralunga sequence, a very detailed description of the seismicity migration was constructed with the help of the multiplets (i.e., clusters of similar events) detected at the PIEI reference station (Fig. 6a) using a cross-correlation threshold of 0.90 (see Appendix A).

The evolution of the migration process was studied considering the sections identified on the supposed structure, one of which corresponds to one or more multiplets. For the sake of simplicity, only 11 multiplets were selected, each of which was composed of more than 10 elements. Figs. 9 and 10 show the evolution in space and time of the migration, both according to the map (along the 307° N direction) and according to the depth, for the period ranging from 5 days before to 35 days after the M_L 3.8 event. Again, for the sake of simplicity, the distances from the main event in Fig. 9 were calculated by projecting the hypocenters on a vertical plane along the 307° N direction. The hypocenters of these seismic events lay across a high-angle plane, and the migration clusters were in proximity to this plane. Thus, the approximate value of the apparent migration velocity calculated on the vertical plane provides a good estimate, taking into account also the uncertainty of the locations.

In general, the migration is characterized by a non uniform trend, although it is strongly driven by the activation of the different multiplets. The migration started with the generation of two multiplets (multiplets 6 and 7), on April 11. These thus occurred, about 4 days before the M_L 3.8 event, and 0.5 km SE of its epicenter, and the migration reached the location of the main event on April 14, a day before it occurred. Multiplet 7 arose at the same time as multiplet 6, and on the map it lies about 300 m over it (Fig. 10). In this period, the apparent average velocity of the migration was 0.17 km/day (see Fig. 9, segment A). A few hours before the main event, two weak earthquakes with M_L 2.3 and 2.1 occurred at different depths; the deeper of these belonged to multiplet 6, whereas the shallow one was an outlier with respect to the waveform similarity. On April 15, 2010, the main event occurred at a depth of 4.67 km (big yellow-red star in Fig.9 and 10), at a depth halfway between multiplets 6 and 7. Over the next few hours, the seismicity moved 0.8 km from the main event epicentre towards NW (see Fig. 9, segment B) and 1.5 km towards the SE, covering

about 1.5 km in depth (Fig. 10). The seismicity towards the NE was described by multiplet 6, wich died in the next 24 h, and by other groups composed of <10 elements (Fig. 9 and 10, black). After this abrupt activity, the seismicity did not migrate again towards the SE (Fig. 9); on the contrary, new multiplets with more than 10 elements appeared towards the NW (families 2, 3, 10, 12); families 2 and 12 were at shallower depths with respect to the main event hypocenter, while families 3 and 10 ranged in depth from about 4 km to 5 km (Fig. 10). Families 10 and 12 did not migrate from the volume covered by the seismicity generated soon after the main event, whereas families 2 and 3 migrated towards the NW during the 2 days after the main event, starting from near families with velocities of 0.18 km/day (see Fg. 9, segment C1) and 0.42 km/day (see Fig. 9, segment C2), respectively. The migration stopped 48 h after the main event. Then during the next 24 h, the seismicity was described by multiplet 25, wich appeared at a depth between 4.25 km and 4.50 km. Abruptly, 72 h after the main event, the migration towards the NW covers about 1 km (see segment D), wich involved events belonging to family 3. Over the next 24 h, 11 events with $M_L \geq 2$ occurred, and the migration followed family 27, to reach the greatest depth of the sequence (6 km). At this point, on the map the migration covered 3.5 km towards the NW, with an average velocity of 0.41 km/day (Fig. 9, from 'a' to 'b'). In the following week, the seismicity was more scattered and the rate of seismicity decreased considerably (Fig. 4, middle panel). In this final period, family 19 characterized the shallowest seismicity, although in a separate cluster that did not belong to the structure described by the migration (purple circles in Fig.7). The last step of the migration is represented by segment F (Fig. 9), in correspondence of which family 37 occurs just beyond family 3 (Fig. 9) and at the same depth (Fig. 10).

The frames of Fig. 11 (symbols for multiplets are the same as given in the legends of Figs. 9 and 10) depict the NW migration of the Pietralunga sequence seismicity. To correlate the seismicity pattern and the kinematics of the events, Fig. 11 also shows the focal mechanisms calculated for the events with $M_L \geq 2$ that are collected in two data bases (Tab. 1): the INGV-CNT-TDMT (based on waveform inversion; Scognamiglio et al., 2009) and the BB (based on first-motion polarities; Monachesi et al., 2012). BB mechanisms are routinely calculated when more than 25 polarities are available. Three further focal mechanisms (Tab. 1, M01, M02 and M30) with more than 20

polarities were calculated for this sequence. In general, the mechanisms are very similar and they highlight normal faulting that is characterized by a NW-SE Apennine direction. In particular, the focal mechanisms calculated for the main event (M03-DTMT) show a fault plane with a strike of 307° and a dip of 61°. Tab. 1 gives the solutions that show a NE dip direction, which are consistent with the deepening highlighted by the seismicity pattern. Table 1 shows strikes that ranged from 295° to 320°, dips that ranged between 55° and 65°, and rakes of around -90° (i.e., pure normal faulting). For mechanism M30 (Tab. 1), the SW-dipping plane was considered, because this earthquake belongs to cluster 2 of Fig. 6 and 7 (purple circles). This was interpreted as a possible antithetic structure with respect to the ATF fault and to the structure depicted by cluster 1, although dealing with just one mechanism and with a cloud geometry of the cluster, we cannot confirm this hypothesis.

Tab.1 reports the mechanisms that are related to both of the events belonging to multiplets 2, 3 and 37 (see 'Family ID' column) and to events not included in multiplets ('X' in the 'Family ID' column).This feature reflects the analysis approach in the detection of the families; we selected the largest part of the earthquake waveform, including the early S phase, to cross-correlate the pairs of events. The similarityof events recorded at PIEI station relative to the cross-correlation threshold of 0.90, is especially due to the energetic wave train of each event, whereas the splitting into different families at higher thresholds is particularly due to the different S-P times, and reflects the different geometrical positions of the events (Fig. 12). Therefore, events belonging to different families (or not belonging to any) can still have similar focal mechanisms.

The N-W-wards migration of the seismicity allowed us to hypothesize the activation of contiguous zones. To support this idea, the seismicity that fills the investigated surface is presented in Fig. 13. The space-time evolution of the seismicity shows the foreshocks, wich belong to two adjacent multiplets that move near the main hypocenter, filling a surface of less than 1 km^2. Their migration finishes with 2 events of M_L >2. The early foreshocks of the main event fill about 3 km^2 around the main hypocentre, and the move towards both the NW and SE in a layer ranging in depth between 4 km and 5 km. Over the next few days, the migration towards NW the at a depth ranging between 4 km and 5 km appeared locked with respect to the lower migration, which reaches 6 km in depth.

The layer from 4 km and 5 km in depth was filled by events that occurred in the period May 2010 - January 2012, as shown in Fig. 2.

6. Discussion

In this study, we investigated the seismic sequence that occurred near Pietralunga (central Italy) in April 2010. The high density of the three-component INGV stations installed in the area allowed the recording of a very high number of micro-earthquakes. In all, 80% of the recorded events ranged in magnitude between 0 and 1; the highest magnitude was 3.8, which was recorded for the April 15, 2010 (01:47 UTC) event. Each recorded waveform was manually picked to carefully detect both P and S arrival-times. The absolute locations (Figs. 1 and 2) were performed using the Hypoellipse code (Lahr, 1979). The cross-correlation lags were calculated at each station on the P and S windows for all of the possible pairs of events, and they were applied to the relative events location, performed using the HypoDD code (Waldhauser and Ellsworth, 2000). The relative locations were performed considering all of the events of the sequence, and these provided a good depiction of the geometry of a fracture system that is characterized by a NW-SE strike (307° N), which corresponds to an Apennine orientation. This strike is exactly perpendicular to the NE trending of the tensional state of stress in the area, as obtained using two regional stress tensors with sub-horizontal σ^3-axis towards 36° N and 39° N (Boncio and Lavecchia, 2000). The hypothesized structure in this study has an extension on the map of 5 km, ranges in depth between 4 km and 6 km, and deepens with an angle of about 65° towards the NE. This structure lies on the hanging wall of the ATF and it is synthetic with respect to its trend (Fig. 7). It is worth noting that in the same area, further studies devoted to the ATF main fault highlighted the presence of seismicity with similar characteristics (Piccinini et al., 2003; Chiaraluce et al., 2007).

The seismicity pattern highlighted in the present study might represent a fragility zone that is located in correspondence to pre-existing fractured rock that is affected by an ancient compressive regime, where brittle behavior is preferred. Indeed, the hanging wall of the ATF is characterized by a high density of fault planes that arose in the framework of an ancient compressive regime that

caused both thickening and horizontal shortening of the sedimentary cover (Mirabella et al., 2008). Considering that the main event of the Pietralunga sequence (Figs. 1, 2, 4) is characterized by a source with limited dimensions (i.e., some hundreds of meters), we cannot affirm that the relocated pattern represents a single fault plane that can potentially slip at the same time. However, our results highlight a seismicity that clearly depicts a NW-SE geometrical plane, on which the events with M_L ≥2 show consistent focal mechanisms. The Apennine main direction (NW-SE) that characterizes both the seismicity pattern and the migration is equally consistent with the strike of the focal mechanisms presented in the present study (307° ±12°) and with the regional fault systems (Chiaraluce et al., 2004, 2007; Mirabella et al., 2011). The topography of the ATF isobaths generally follows this strike (Fig. 1). These observations agree with the forces that drive the ATF during the reactivation of the fault systems on the hanging wall, as expressed through the background seismicity of the area and/or low energy seismic sequences, such as that investigated in present study study.

The April 2010 Pietralunga sequence was confined between 4 km and 6 km in depth. In this area, the isobaths of the ATF ranged between 6 km and 7 km (see Figs. 6 and 7). As recently hypothesized in other studies (Chiaraluce et al., 2004, 2007), this feature is probably responsible for the cut-off of the seismicity that has already been observed during other seismic sequences that occurred in this sector of the Apennines: Valnerina 1979 (Deschamps et al., 1984), Gubbio 1984 (Haessler et al., 1988), Umbria-Marche Apennines 1997 (Amato et al., 1998). Furthermore, the ATF low-angle normal fault represents a detachment for the complex high-angle synthetic splays that have been mapped on the surface (Mirabella et al., 2011). Mirabella et al. (2011) presented two geological sections of the crust (S1, S3 therein) obtained by integrating the surface geological information with the geological interpretation of seismic lines and Vp data from boreholes, with NW and SE trends, respectively, with respect to the Pietralunga sequence (Fig. 14). The sections depict the ATF extensional system, with the complex structure on its hanging wall in the eastern part of the sections. The S1 geological section (Fig. 14) is NW of the Pietralunga sequence, and it shows the Evaporites layer at a depth of 4 km to 6 km, on the hanging wall of the ATF, whereas the S3 section (SE of the Pietralunga sequence) shows the top

of the basement or the Evaporites layer at the same depths. If we take into account the complex trend of deepening that characterizes the ATF plane towards the SE, the location of the Pietralunga sequence is consistent with the Evaporites layer.

The lithology of the Evaporites is composed of a series of anhydritic and dolomitic layers (Anelli et al., 1994; Ciarapica and Passeri, 1976; Ciarapica and Passeri 1980; Ghelardoni, 1962; Martinis and Pieri, 1964). Tests relating to the elasticity properties of the anhydrites and dolomites have indicated different limits of the brittle deformations (Bell, 1994; Handin and Hager, 1957; Mirabella, 2002; Mogi, 1971; Mueller and Siemes, 1974): ≤100 MPa and ≥200 MPa respectively. As a confining pressure of 150 MPa to180 MPa is expected at a depth of 6 km, Mirabella et al. (2008) suggested that evaporites are mechanically dominated by dolomites: then the evaporitic layer has a brittle behavior and the release of stress from its clouds affects the faulting of the overhanging carbonates that arises. This hypothesis might also be supported by the presence of deep over-pressured fluids (Chiodini et al., 2000; Miller et al., 2004; Trippetta et al., 2013), as happened for the Umbria-Marche Apennine 1997 moderate earthquakes (Chiaraluce et al., 2003; Miller et al., 2004). The Triassic Evaporites might have an important role in the trapping of fluids, due to the exceptionally low permeability at elevated pressure of the anhydrite (Trippetta et al., 2010). Moreover, the anhydrite (Ca-sulfate layers) maintains a low permeability even during deformation, as this manner of deformation is ductile rather than brittle (De Paola et al., 2009; Trippetta et al. 2013). These features are observed in outcrop exposures of the Evaporites that show fluid-assisted pervasive fractures in dolostones, unlike the Ca-sulfate layer (Trippetta et al. 2013). The trapping of fluid was observed in the Pieve Santo Stefano borehole stratigraphic log (about 30 km NW of the Pietralunga sequence), where overpressured CO_2 fluid lies within dolostones (i.e., the reservoir layers) between anhydrites (i.e., the sealing layers) at depths >3.5 km (Trippetta et al., 2013). The stratigraphic logs indicate up to decametric continuous portions of dolostones, whereas the field data show localized displacements of up to hundreds of meters of brittle faults, probably favored by the presence of dolostones (Trippetta et al., 2013). The separate fluid reservoirs in dolostones are linked by these faults (Fig. 14b) which represent a way for fluid flow at the crustal scale (Collettini et al., 2009). The low magnitude of the events released during the Pietralunga

sequence and the jerky migration of the seismicity investigated might be due to a flow of fluids into the Evaporitic layer. The spatial and temporal distribution of the seismicity that was calculated on absolute locations is consistent with the diffusion process of the relaxation pressure (Amato et al., 2010).

The high resolution of the recorded seismicity, the relative location procedures, and the detection of multiplets provide us with a very detailed description of the seismicity migration. The migration moves along its path with an apparent mean velocity of 0.4 km/day (Fig. 9), which is in general lower compared to the values observed during recent sequences recorded in central Italy (e.g., 1 km/day for the Mw 6.0 Umbria-Marche Apennine 1997 sequence, Catalli et al., 2008; 3.5 km/day for the Mw 6.3 L'Aquila 2009 sequence, Chiaraluce et al., 2011). In any case, the fast span of the seismicity after the main event and 3 days later (Fig. 9, segment B, D, respectively) contributes to the approximated value of the velocity migration, which is an upper limit with respect to the apparent velocity of the detailed slices of the migration (Fig.9, segments A, C1, C2, E). The M_L 3.8 event that occurred on April 15, 2010, triggered a seismicity that spanned 2.5 km in 24 h (Fig. 9) and covered a surface of about 3 km^2 (34.7 m^2/s) (Fig. 13c). As well as the jerky shape, the migration towards the NW was characterized by two branches, both stemming from the hypocenter of the main event. The first branch moved upwards and then stopped after 1.5 km; further on, the rate of events quickly decreased in time and there were few events per day for this portion of migration. The second branch moved downwards and the migration front proceeded 4 km towards the NW (Fig. 13). Then, in our case, the migration was composed of steps represented by different processes, which were probably mainly characterized by fluid flow and brittle deformation that resulted in the extensional system accommodated by the aseismic slip (Chiaraluce et al., 2007) of ATF low-angle normal fault. The anisotropic behavior of the migration might be due to the complex architecture of the fault system that characterizes the hanging wall of the ATF, and to the heterogeneity of the mechanical behavior that characterizes some of the lithological components of the Evaporites. All of the variables of the complex geological system contribute to the migration process that we observed in detail through relocation procedures and multiplet detection. In particular, the multiplet detection allowed us to describe another important feature of the migration:

the triggering of contiguous patches on the plane of the seismicity pattern. This behavior agrees with the structure and characteristics of the Evaporites where the porosity of fractured dolostones increases due to deformation and following cracking, and fluid reservoirs are linked by brittle faults (Trippetta et al., 2013). We hypothesize the start of the Pietralunga sequence in the dolostone reservoir, with two contiguous multiplets that reached and perturbed the area of the mainshock. The mainshock fractured the surrounding volume, increased the permeability, and probably linked dolostone patches where fluids can flow. Next, the multiplets began from the source of the main event and migrated towards the NW. The migration did not show any drop in the space; each patch of the pattern was filled up if it was previously affected by seismicity that occurred very close by (Fig. 13).

Finally, it is interesting to note that the direction of migration (about 307° N) is perpendicular to the tensional state of stress and it matches the mean of the fast polarization directions of the seismic anisotropy. Pastori et al. (2012) calculated the anisotropic parameters by shear-wave splitting in the ATF area at 13 stations that belong to the so-called “Città di Castello experiment” (Piccinini et al., 2003). They obtained a dominant NW-SE fast polarization direction that was parallel to the strikes of major faults exposed in the area. These features were confirmed by the preliminary results of the anisotropic parameters calculated for Pietralunga sequence (Guerri et al., 2012), where the fast polarization directions were parallel to the maximum horizontal stress. The alignment of fluid-filled micro-cracks parallel to the maximum horizontal stress is considered the principal cause of shear-wave splitting (Crampin and Peacock, 2008). The increase in crack density causes coalescence of micro-cracks up to a critical point that causes fracture field variations and triggers greater fractures (Crampin, 1993). In our case, the maximum horizontal stress of the area and the fracture alignments contributed to the spreading of a preferred way for the seismicity migration along the observed strike direction.

7. Conclusions

We have described here the detailed pattern and migration of a seismic sequence that occurred near Pietralunga, a small town in the central Apennines (Italy). On April 2010, about 1400 events were recorded by the dense, high-resolution seismic networks managed by INGV. The absolute arrival times obtained from the manual picking of the P-phases and S-phases, and the relative ones obtained from cross-correlations, were used to relocate the seismic sequence with the double difference algorithm implemented in the HypoDD code (Waldhauser and Ellsworth, 2000). The relocation depicted a seismicity pattern that described a structure that was 5 km long and 2 km thick, dipping towards the NE. The focal mechanisms calculated from the events with $M_L \geq 2$ are consistent with the structural geometry highlighted by the Pietralunga sequence. This evidence agrees with the opinion that the seismicity of this sequence lies on a single plane, which is slightly curved towards the NW on the map, and which is characterized by a common regime. The structure is synthetic with respect to the ATF low-angle normal fault, and it lies on its hanging wall. The seismicity appears to be just above the ATF; thus our data confirm a clear separation between an aseismic footwall and an active hanging wall (Chiaraluce et al., 2007).

The details of the seismicity migration were deduced by analyses based on multiplet detection. The migration moved towards the NW along the hypothesized structure, following the NW direction of the Apennines. At the end of each multiplet, one or more multiplets arose and covered an adjacent surface, involving the previous seismicity that had just occurred in time. What the first triggering mechanism of micro-seismicity that occurred during the Pietralunga sequence was remains an open issue. The hypocenters are mainly located between 4 km and 6 km in depth, and they are probably confined to the Triassic Evaporite layer. The triggered seismicity that was observed during the migration process supports the hypothesis of fluid flows into the dolostone layers of the Evaporites, which is favored by the normal brittle deformation of the ancient structures involved in the early compressive phases or of new fractures that evolved due to the tensional state of the stress in the area.

The complex fault system of the ATF hanging wall (Mirabella et al., 2011) and the different mechanical behaviors of the Evaporites (Mirabella et al., 2008; Trippetta et al., 2010; Trippetta et al., 2013) can explain the asymmetric shape of the migration observed in the present study. The

brittle deformation during the main events of the Pietralunga sequence probably links the different dolostone reservoirs and fluids, and can flow through their intense fracturation, aligned in the maximum horizontal stress direction.

It also remains to be understood whether the structure highlighted by the Pietralunga sequence can break at the same time, wich would result in an important earthquake. Indeed, in correspondence to the ATF fault system, moderate earthquakes have occurred in the shallow brittle crust over the last few decades. Thus, the occurrence of complex micro seismic sequences indicates the importance of continuous and detailed monitoring of the ATF area, to improve our knowledge of the seismic hazard of the investigated sector and of the preparatory phase of moderate earthquakes.

Appendix A

The recognition and grouping together of seismic events with similar characteristics (e.g., very close locations, similar waveforms, common focal mechanism) can be a useful tool for seismotectonic studies, to define the seismicity behavior of buried and poorly known active structures.

Often, events of this kind are recognized during seismic sequences, as episodes that produce a release of energy that is spread over a great number of earthquakes that occur before or after a mainshock. Such phenomena are close in space and time, and are characterized by repeated breaks that can propagate from the main fracture towards the surrounding brittle volumes. Generally, the preliminary event locations highlighta cloud of hypocenters, known as a cluster of events.

When a seismic sequence is analyzed in detail, it is common to find events that, as well as being located close to each other, also show high levels of waveform similarity at the same recording station. Such events are commonly defined as doublets (as pairs) or multiplets (when in a series). Doublets and multiplets include events where the hypocenters lie within one quarter of a dominating wavelength from each other (Geller and Mueller, 1980) and the occurrence of which is

caused by repeated breaks in the same asperity, thereby generating energy release due to subsequent slip on the same fault plane during foreshock-mainshock-aftershock sequences. In this context, and as demonstrated in many studies (e.g., Deichmann and Garcia-Fernandez, 1992; Geller and Mueller, 1980; Tsujura, 1983) the analyzed earthquakes are generated by sources that show very similar focal mechanisms.

The main difference between a cluster and a multiplet depends on the level of knowledge of the phenomenon: a cluster describes a qualitative idea based on the spatial distribution of the hypocenters, while a multiplet represents a quantitative idea based on the level of waveform similarity of the earthquakes analyzed.

In the case of a detailed study that includes a large number of earthquakes that are very close to each other in space, the routine location procedures (e.g. absolute hypoellipse location, Lahr 1979) can be sensitive to many factors that can cause significant errors in the determination of the hypocenters: uncertainties in the automatic phase picking, particularly for the S-phase onset, which is essential to constrain the hypocentral depth; subjectivity of the operator during manual picking; uncertainties in seismic-phase recognition due to an insufficient signal-to-noise ratio at some of the recording stations; uncertainties in the crustal velocity model; low numbers of phases avalaible; and unfavorable network geometry with respect to the seismicity investigated.

All of these factors can occasionally lead to location errors that are larger than the dimension of the investigated source. During detailed seismic sequence analyses (particularly when the geological background of the investigated fault is not available), possible bias derived from the ordinary location procedures, is overcome by refining the hypocenter coordinates with the relative location methods. Supposing that(i) the hypocentral separation of two earthquakes is negligible if compared to the single event-station hypocentral distance, and

(ii) the travel-times between the source area and a common receiver are similar along the entire ray-paths, it can be assumed that the travel-time difference between a pair of events is due to the spatial offset between them (Fréchet, 1985; Frémont, 1984; Poupinet *et al.*, 1985; Scarfì et al., 2003).

To move from a cluster to a multiplet a waveform similarity analysis is needed. Several methods have been developed: cross-spectral techniques (Got et. al., 1994; Scherbaum and Wendler, 1986), pattern recognition (Joswig, 1995), a fractal approach (Smalley et al., 1987), syntactic pattern-recognition schemes (Zhinzhin et al., 1992; 1994), non-linear correlation technique (Schulte-Theis and Joswig, 1993), and dendrogram analysis (Schulte-Theis, 1995).

To detect similarities among the recorded events, we applied a cross-correlation technique (e.g. Augliera et al., 1995; Cattaneo et al., 1997, 1999; Ferretti et al., 2005; Massa et al., 2006a, 2006b). Given two events *a1* and *a2* recorded at the same station, it is possible to compute a very accurate estimation of the difference in the arrival times, with respect to a common time reference, by using the cross-correlation function:

$$C_{12}(\tau) = \int_{-\infty}^{+\infty} [a1(t)\ a2(t+\tau)]\ dt \qquad (A.1)$$

For the computation, it is neither necessary nor recommended to use the whole signals, but just a significant part of them. For a comparison, some seconds selected on each seismogram are analyzed, with the provision that the selected portion has to be representative of the source of the event. Assuming that two considered events have a quasi-identical transient time history that is simply shifted in time (as here)

$$a_2(t) = a_1(t-\tau') \qquad (A.2),$$

with superimposed uncorrelated random noise, a quasi-autocorrelation of the signal is expected as a result. In the case of signals with a strong transient character, the correlation function shows a narrow bell-shape around its maximum. Moreover the coherent part of the signals can be enhanced by applying appropriate filtering.

The cross-correlation analysis is performed considering a reference station. In particular, high values of similarity at a single station are a sufficient condition, because the aim is to detect the same source for different events; indeed, the similarity might be impaired by propagation,

attenuation, site effect and several factors (e.g., instrumental limitation, occurrence of strong incoherent noise, superposition of different events very closely spaced in time, etc., Cattaneo et al.,1997).

The search for waveform similarity is carried out by constructing a matrix that contains the maximum value of the normalized cross-correlation for all of the analyzed pairs of events. The advantage of this approach is the possibility to include in the cross-correlation matrix not only the events that strictly belong to a particular seismic sequence but also isolated events that occurred in the area of interest at a different time (i.e. temporal multiplets, Augliera et al., 1995).

Once the output of the cross-correlation matrix is available, a minimum threshold of similarity has to be *a-priori* (and arbitrarily) imposed to group the analyzed events in multiplets. The cross-correlation coefficient among events ranges from 0 for completely different waveforms to 1 for waveforms that are clones (i.e. autocorrelation).

In the present study, to gather the events into families, we applied the bridging technique that as been proposed in many studies (e.g., Aster and Scott, 1993; Cattaneo et al. 1997, 1999; Deichmann and Garcia-Fernandez, 1992; Ferretti et al., 2005; Massa et al., 2006a). In general, this approach allows the problem of comparing events with different magnitudes to be avoided. The bridging technique is based on the equivalence class algorithm (Press et al., 1988), which is, in turn, based on the principle that if two pairs of events (*a1*,*a2*) and (*a2*,*a3*) share a common quake (*a2*), then all three events are attributed to the same multiplet, even if the match between *a1* and *a3* is below the selected threshold for similarity: in this case, the event *a2* acts as the *bridge* event between the pairs.

The Pietralunga sequence was recorded by a relevant number of stations installed in the area (Fig. 1, red). To select a reference station, the cross-correlation matrix wasinitially calculated at some receivers considering the waveforms of the vertical component filtered between 1 Hz and 10 Hz. In all cases, the windows of signal that allowed us to consider a portion of the P-phases and S-phases were selected. Indeed, while the inspection of the S train waves can assure high sensitivity at the ray path (i.e. the S waves are merely affected by the propagation, which, in a highly heterogeneous area, can hardly be reproduced by chance; Cattaneo et al., 1999), the first pulses

of the P-phase, which is more influenced by the radiation pattern, can easily be reproduced also by events located in different positions. In some cases, the decrease with increasing distance for the similarity detected for the P-phase might be due to the attenuation effects (e.g., geometrical spreading and anelastic attenuation) involving the high frequency components of the signals (Morasca et al., 2006).

Considering: (i) the highest number of recorded events (about 1500); (ii) the good signal-to-noise ratio obtained from both P-phases and S-phases; (iii) the short distance with respect to the epicentral area (about 20 km);(iv) the transversal position with respect to the main elongation of the sequence (see Fig. 1), PIEI was chosen as a reference station. Fig. A.1 shows the cross-correlation matrix that was deduced from the selected station.

After the calculation of the cross-correlations at the reference station, and the subsequent application of the bridging technique to the values obtained from the matrix, the last problem to solveto group the events into multiplets is the setting of a minimum cross-correlation threshold.

The cross-correlation threshold (i.e., index of waveform similarity) is chosen by a two-step procedure (see, for instance, Cattaneo et al., 1997, 1999; Ferretti et al., 2005; Maurer and Deichmann, 1995). First, the Gaussian representing the distribution of the cross-correlation coefficients obtained from all of the pairs of events recorded by the reference station is analyzed by simple visual inspection. The minimum threshold is selected where the plot shows a sudden flattening and the trend deviates from a pure normal distribution (Massa et al., 2006b; Maurer and Deichmann, 1995): in our case the histogram reported in Fig. A.2 indicates that for PIEI station, this happens around a value of 0.6.

Then, considering the minimum value detected by the previous step, increasing thresholds are examined to find the value that assures at the same time the highest number of multiplets and, on average, the highest number of components per multiplet. In our case, if thresholds lower than 0.85 are considered, we find a very large multiplet that includes hundreds of elements and, in practice, most of the investigated sequence (Fig. A.3). The sequence appears to be fragmented reaching the threshold of 0.90; in this case several families show more than 10 elements.

Increasing the threshold again to 0.95, the result that is obtained has no real meaning because a very high number of micro multiplets (number of elements ≤3) appears.

Acknowledgements

These research activities undertaken with the data collected by the Alto Tiberina Seismic Network (ATSN) were carried out within the TABOO (The Alto tiBerina near fault ObservatOry, http://taboo.rm.ingv.it) working group, which is coordinated by Lauro Chiaraluce. The ATSN was created through funding provided by the Airplane (FIRB-MIUR), GLASS (ERC-EU), NERA (EU) and MOLE (ICDP) projects, which are coordinated by Alessandro Amato, Cristiano Collettini, Alberto Michelini and Massimo Cocco.

We acknowledge the anonymous reviewers for their constructive and helpful reviews, L. Chiaraluce for helpful suggestions and discussions on seismological aspects, V. Castelli and C. Berrie for reading and improving the manuscript text, and all of the people that assure the functionality of the INGV seismic networks.

References

Alvarez, W., 1972. Rotation of the Corsica-Sardinia microplate. Nature 248, 309–314.

Amato, A., Azzara, R., Chiarabba, C., Cimini, G.B., Cocco, M., Di Bona, M., Margheriti, L., Mazza, S., Mele, F., Selvaggi, G., Basili, A., Boschi, E., Courboulex, F., Deschamps, A., Gaffet, S., Bittarelli, G., Chiaraluce, L., Piccinini, D., Ripepe, M., 1998. The 1997 Umbria-Marche, Italy earthquake sequence: A first look at the main shocks and aftershocks. Geophys. Res. Lett. 25, 2861–2864.

Amato, A., Braun, T., Cattaneo, M., Chiaraluce, L., Cocco, M., D'Alema, E., Di Stefano, R., Frapiccini, M., Latorre, D., Marzorati, S., Monachesi, G., Moretti, M., Piana Agostinetti, N., Piccinini, D., Saccorotti, G., Valoroso, L., 2010. Shallow seismicity migration in a normal fault test

site in northern Apennines (Italy). S21B-2036 Poster Session, AGU Fall Meeting, San Francisco, California, 13-17 December 2010.

Amato, A., Mele, F., 2008. Performance of the INGV National Seismic Network from 1997 to 2007, Annals Geophys., 51, 2-3, 417-431.

Ambrosetti, P., Carboni, M.G., Conti, M.A., Costantini, A., Esu, D., Gandin, A., Girotti, O., Lazzarotto, A., Mazzanti, R., Nicosia, U., Parisi, G., Sandrelli, F., 1978. Evoluzione paleogeografica e tettonica dei bacini tosco-umbro-laziali nel Pliocene e nel Pleistocene inferiore. Mem. Soc. Geol. Ital. 19, 573–580.

Anelli, L., Gorza, M., Pieri, M., Riva, M., 1994. Subsurface well data in the northern Apennines (Italy). Mem. Soc. Geol. Ital. 48, 461–471.

Antonioli, A., Piccinini, D., Chiaraluce, L., Cocco, M., 2005. Fluid flow and seismicity pattern: Evidence from the 1997 Umbria-Marche (central Italy) seismic sequence, Geophys. Res. Lett., 32 L10311, doi: 10.1029/2004GL022256

Aster, R.C., Scott, J., 1993. Comprehensive characterization of waveform similarity in microearthquake data set. Bull. Seismol. Soc. Am 83, 1307-1314.

Augliera, P., Cattaneo, M., Eva, C., 1995. Seismic multiples analysis and its implication in seismotectonics. Tectonophysics 248, 219-234.

Bally, A., Burbi, L., Cooper, C., Ghelardoni, R., 1986. Balanced sections and seismic reflection profiles across the central Apennines. Mem. Soc. Geol. Ital. 35, 257–310.

Barchi, M., Pauselli, C., Chiarabba, C., Di Stefano, R., Federico, C., 2006. Crustal structure, tectonic evolution and seismogenesis in the Northern Apennines (Italy). Boll. Geofis. Teor. Appl. 47, 3, 249–270.

Barchi, M., De Feyter, A., Magnani, M., Minelli, G., Pialli, G., Sotera, B., 1998a. Extensional tectonics in the Northern Apennines (Italy): Evidence from the CROP03 deep seismic reflection line. Mem. Soc. Geol. Ital. 52, 528–538.

Barchi, M., Minelli, R., Pialli, G., 1998b, The crop 03 profile: A synthesis of results on deep structures of the northern Apennines. Mem. Soc. Geol. Ital. 52, 383–400.

Bell, F., 1994. A survey of the engineering properties of some anhydrite and gypsum from the north and midlands of England. Eng. Geol. 38, 1–23.

Boncio, P., Brozzetti, F., Lavecchia G., 2000. Architecture and seismotectonics of a regional low-angle normal fault zone in central Italy. Tectonics 19, 1038–1055.

Boncio, P., Lavecchia, G., 2000. A geological model for the Colfiorito earthquakes (September–October 1997, central Italy). J. Seismol. 4, 345-356.

Catalli, F., Cocco, M., Console, R., Chiaraluce, L., 2008. Modeling seismicity rate changes during the 1997 Umbria-Marche sequence (central Italy) through a rate- and state-dependent model, J. Geophys. Res. 113, B11301, doi:10.1029/2007JB005356.

Cattaneo, M., Augliera, P., Spallarossa, D., Lanza, V., 1999. A waveform similarity approach to investigate seismicity patterns. Natural Hazard 19, 123-138.

Cattaneo, M., Augliera P., Spallarossa, D., Eva, C., 1997. Reconstruction of seismogenetic structures by multiples analysis: an example of Western Liguria, Italy, Bull. Seismol. Soc. Am. 87, 971-986.

Chiaraluce, L., Valoroso, L., Piccinini, D., Di Stefano, D., De Gori, P., 2011. The anatomy of the 2009 L'Aquila normal fault system (central Italy) imaged by high resolution foreshock and aftershock locations. J. Geophys. Res. 116, B12311, doi:10.1029/2011JB008352.

Chiaraluce, L., Chiarabba, C., Collettini, C., Piccinini, D., Cocco, M., 2007. Architecture and mechanics of an active low-angle normal fault: Alto Tiberina Fault, Northern Apennines, Italy, J. Geophys. Res. 112, B10310, doi:10.1029/2007JB005015.

Chiaraluce, L., Amato, A., Cocco, M., Chiarabba, C., Selvaggi, G., Di Bona, M., Piccinini, D., Deschamps, A., Margheriti, L., Courboulex, F., Ripepe, M., 2004. Complex normal faulting in the Apennines Thrust and fold belt: The 1997–1998 seismic sequence in central Italy. Bull. Seismol. Soc. Am., 94, 1, 99–116.

Chiaraluce, L., Ellsworth, W.L., Chiarabba, C., Cocco, M., 2003. Imaging the complexity of an active complex normal fault system: The 1997 Colfiorito (central Italy) case study. J. Geophys. Res., 108, B6, 2294, doi:10.1029/2002JB002166.

Chiodini, G., Frondini, F., Cardellini, C., Parello, F., Peruzzi, L., 2000. Rate of diffuse carbon dioxide earth degassing estimated from carbon balance of regional aquifers: The case of central Apennines, Italy, J. Geophys. Res. 105, B4, 8423–8434.

Ciarapica, G., Passeri, L., 1980. Contributions on evaporites diagenesis, Geol. Mediterr. 7, 1, 43-48.

Ciarapica, G., Passeri, L., 1976. Deformazioni da fluidificazione ed evoluzione diagenetica della formazione evaporitica di burano. Boll. Soc. Geol. Ital. 95, 1175–1199.

Collettini, C., Barchi M.R., 2002. A low angle normal fault in the Umbria region (central Italy): A mechanical model for the related microseismicity. Tectonophysics 359, 97–115.

Collettini, C., Chiaraluce, L., 2013. Integrated laboratories to Study Aseismic and Seismic Faulting. Eos, 94, 10, 97-98.

Collettini, C., De Paola, N., Faulkner, D.R., 2009. Insights on the mechanics of the Umbria–Marche earthquakes (Central Italy) from the integration offield and laboratory data. Tectonophysics 476, 99–109. 10.1016/j.tecto.2008.08.013.

Crampin, S., 1993. Arguments for EDA. Can. J. Explor. Geophys. 29, 18-30.

Crampin, S., Peacock, S., 2008. A review of the current understanding of shear-wave splitting and common fallacies in interpretation. Wave Motion 45, 675-722.

Deichmann, N., Garcia-Fernandez, M., 1992. Rupture geometry from high-precision relative hypocentre locations of microearthquake clusters. Geophys. J. Int. 110, 501-517.

Delladio, A., 2011. Monitoraggio sismico del territorio nazionale. I° Workshop tecnico: Monitoraggio sismico del territorio nazionale: stato dell'arte e sviluppo delle reti di monitoraggio sismico. A cura di Marco Cattaneo e Milena Moretti. Miscellanea INGV, 10, 11-16 (in italian).

De Luca, G., Cattaneo, M., Monachesi, G., Amato, A., 2009. Seismicity in Central and Northern Apennines integrating the Italian national and regional networks, in Tondi, E., Chiaraluce, L.,

Roberts, G. (Eds.), The years after the Umbria-Marche earthquake, Central Italy. Tectonophysics special issue 476, 121–135.

De Paola, N., Faulkner, D.R., Collettini, C., 2009. Brittle versus ductile deformation as the main control on the transport properties of low-porosity anhydrite rocks. Journal of Geophysical Research 114, B06211. http://dx.doi.org/10.1029/2008JB005967.

Deschamps, A., Iannaccone, G., Scarpa, R., 1984. The Umbrian earthquake (Italy) of 19 September 1979, Ann. Geophys. 2, 1, 29–36.

Ferretti, G., Massa, M., Solarino, S., 2005. An improved method for the recognition of seismic families: Application to the Garfagnana–Lunigiana area (Italy). Bull. Seismol. Soc. Am. 95, 5, 1903-1915.

Fréchet, J., 1985. Sismogenese et doublets sismiques. Ph.D. Thesis, University of Grenoble

Frémont, M. J., 1984. Mesure de variations temporelles des paramètres de la croute terrestre et d'effects de sources par traitement de doublets de sèismes. Ph.D. Thesis, University of Grenoble

Geller, R.J., Mueller, C.S., 1980. Four similar earthquakes in central California. Geophys. Res. Lett. 7, 821-824.

Ghelardoni, R., 1962. Stratigrafia e tettonica del Trias di M.Malbe presso Perugia. Boll. Soc. Geol. Ital. 81, 66–75.

Got, J., Fréchet, J., Klein F.W., 1994. Deep fault plane geometry inferred from multiplet relative relocation beneath the south flank of Kilauea. J. Geophys. Res. 99, 15375-15386.

Guerri, M., Pastori, M., Margheriti, L., D'Alema, E., Piccinini, D., Barchi, M.R., 2012. Seismic anisotropy and micro-seismicity in the upper crust at north of Gubbio basin (Central Italy): relation with the subsurface geological structures and the active stress field. 31° ConvegnoGruppo Nazionale di Geofisica della Terra Solida, T1 S1.1, Potenza, 20-22 November 2012.

Haessler, H., Gaulon, R., Rivera, L., Console, R., Frogneux, M., Gasparini, G., Martel, L., Patau, G., Siciliano, M., Cisternas, A., 1988. The Perugia (Italy) earthquake of 29 April 1984: A microearthquake survey. Bull. Seismol. Soc. Am. 78, 1948–1964.

Handin, J., Hager, R., 1957. Experimental deformation of sedimentary rocks under confining pressure: tests at room temperature on dry samples. Bull. Am. Assoc. Pet. Geol., 41, 1, 1–50.

Jolivet, L., Faccenna, C., Goffé, B., Mattei, M., Rossetti, F., Brunet, C., Storti, F., Funiciello, R., Cadet, J.P., d'Agostino, N., Parra, T., 1998. Midcrustal shear zones in postorogenic extension: Example from the northern Tyrrhenian Sea. J. Geophys. Res. 103, 12,123–12.

Joswig, M., 1995. Automated classification of local earthquake data in the BUG small array, Geophys. J. Int. 120, 262-286.

Lahr, J.C., 1979. Hypoellipse: a computer program for determining local earthquake parameters, magnitude, and first motion pattern, U.S. Goel. Surv., Open File Rep. 79-431.

Martinis, B., Pieri, M., 1964. Alcune notizie sulla formazione evaporitica dell'Italia centrale e meridionale. Mem. Soc. Geol. Ital. 4, 649 – 678.

Massa, M., Eva, E., Spallarossa, D., Eva, C., 2006a. Detection of earthquake clusters on the basis of waveforms similarity: An application in the Monferrato region (Piemonte, Italy). J. Seism. 10, 1-22

Massa, M., Ferretti, G., Spallarossa, D., Eva C., 2006b. Improving automatic location procedure by waveform similarity analysis: An application in the south western Alps (Italy), Phys. Earth Planet. 154, 1, 18-29.

Maurer, H., Deichmann, N., 1995. Microearthquake cluster detection based on waveform similarities, with an application to the western Swiss Alps. Geophys. J. Int. 123, 588-600.

Miller, S., Collettini, C., Chiaraluce, L., Cocco, M., Barchi, M., Klaus, B., 2004. Aftershocks driven by a high pressure CO2 source at depth. Nature, 427, 724–727.

Mirabella, F., Brozzetti, F., Lupattelli, A., Barchi, M.R., 2011. Tectonic evolution of a low-angle extensional fault system from restored cross-sections in the Northern Apennines (Italy). Tectonics, 30, TC6002, doi:10.1029/2011TC002890

Mirabella, F., Barchi, M., Lupattelli, A., Stucchi, E., Ciaccio, M., 2008. Insights on the seismogenic layer thickness from the upper crust structure of the Umbria-Marche Apennines (central Italy). Tectonics, 27, TC1010, doi:10.1029/2007TC002134.

Mirabella, F., 2002. Seismogenesis of the Umbria-Marche region (Central Italy): Geometry and kinematics of the active faults and mechanical behaviour of the involved rocks, Ph.D. thesis, Univ. of Perugia, Perugia, Italy.

Mogi, K., 1971. Effect of the triaxial stress system on the failure of dolomite and limestone. Tectonophysics, 11, 111–127.

Monachesi, G., Cattaneo, M., 2010. La dorsale radio Wi-Fi per il monitoraggio multiparametrico in Alta Val Tiberina. Rapporti Tecnici INGV, 129.

Monachesi, G., Cattaneo, M., Ladina, C., Marzorati., S., D'Alema, E., Frapiccini, M., Carannante, S., Ferretti, M., Sebastianelli, M., Delladio, A., Selvaggi, G., 2013. Experiences of integrated monitoring; the case of Central Eastern Italy seismic network and its services. Quaderni di geofisica, 106, 1-29 (in Italian).

Morasca , P., Malagnini, L., Akinci, A., Spallarossa, D., 2006. Ground motion scaling in the Western Alps. J Seismol, 10, 3, 315–333

Mueller, P., Siemes, H., 1974. Festigkeit, verformbarkeit und gefuegeregelung von anhydrit—Experimentelle stauchverformung unter manteldrucken bis 5 kbar bei temperaturen bis 300 c. Tectonophysics, 23, 105–127.

Noir, J., Jacques, E., Be`kri, S., Adler, P.M., King,G.C.P., 1997, Fluid flow triggered migration of events in the 1989 Dobi earthquake sequence of Central Afar. Geophys. Res. Lett. 24, 2335–2338.

Pacchiani, F, Lyon-Caen, H., 2009, Geometry and spatio-temporal evolution of the 2001 Agios Ioanis earthquake swarm (CorinthRift,Greece), Geophys. J. Int. , 180, 1, 59-72. doi:10.1111/j.1365-246X.2009.04409.x.

Pastori, M., Piccinini, D., Valoroso, L., Wuestefeld, A., Zaccarelli, L., Bianco, F., Kend All, J.M., Di Bucci, D., Margheriti, L., Barchi, M.R., 2012. Crustal fracturing and presence of fluid as revealed by seismic anisotropy: case histories from seismogenic areas in the Apennines (Italy). Bollettino di Geofisica Teorica ed Applicata 53, 4, 417-433.

Pialli, G., Barchi, M., Minelli, G., 1998. Results of the CROP03 deep seismic reflection profile Mem. 52. Soc. Geol. Ital. Ed., Rome.

Piccinini, D., Cattaneo, M., Chiarabba, C., Chiaraluce, L., Demartin, M., Di Bona, M., Moretti, M., Selvaggi, G., Augliera, P., Spallarossa, D., Ferretti, G., Michelini, A., Govoni, A., Di Bartolomeo, P., Romanelli, M., Fabbri, J., 2003. Microseismic study in a low seismicity area of Italy: The Città di Castello 2000 – 2001 experiment. Ann. Geophys. 46, 6, 1315–1324.

Poupinet, G., Fréchet, J., Ellsworth, W.L., Frémont, M.J., Glangeaud, F., 1985. Doublet analysis: improved accuracy for earthquake prediction studies. Earthquake Predict. Res. 3, 147-159.

Press, W.H., Flannery, P.B., Teukolsky, S.A., Wetterling, W.T., 1988. Numerical Recipes in C, The art of Scientific computing. Cambridge University Press, Cambridge, UK.

Reutter, K.J., Giese, P., Closs, H., 1980. Lithospheric split in the descending plate: Observations from the northern Apennines. Tectonophysics, 64, T1– T9.

Salvaterra, L., Pintore, S., Badiali, L., 2008. Rete sismologica basata su stazioni GAIA. Rapporti Tecnici INGV, 68.

Scarfì, L., Langer, H., Gresta, S., 2003. High-precision relative locations of two microearthquake clusters in Southeastern Sicily, Italy. Bull. Seismol. Soc. Am. 93, 1479-1497.

Schulte-Theis, H., 1995. Cluster analysis of European seismicity. Cahiers du Centre Européen de Géodynamique et de Séismologie 12, 201-224.

Schulte-Theis, H., Joswig, M., 1993. Clustering and location of mining induced seismicity in the Ruhr basin by automated master event comparison based on dynamic waveform matching (DWM). Comput. Geosci. 19, 233-242.

Scognamiglio, L., Tinti, E., Michelini, A., 2009. Real-Time determination of seismic moment tensor for italian region. Bull. Seism. Soc. of Am. 99, 4, 2223-2242.

Sherbaum, F., Wendler, J., 1986. Cross spectral analysis of Swabian Jura (SW Germany) three component microearthquake recordings. J. Geophys. 60, 157-166.

Smalley, R.F., Chatelain, J.L., Turcotte, D.L., Prévot, R., 1987. A fractal approach to the clustering of the earthquakes: applications to the seismicity of the New Hebrides. Bull. Seismol. Soc. Am. 77, 1368-1381.

Trippetta, F., Collettini, C., Vinciguerra, S., Meredith, P.G., 2010. Laboratory measurements of the physical properties of Triassic Evaporites from Central Italy and correlation with geophysical data. Tectonophysics 492, 121–132. 10.1016/j.tecto.2010.06.001.

Trippetta, F., Collettini, C., Barchi, M.R., Lupattelli, A., Mirabella, F., 2013. A multidisciplinary study of a natural example of a CO2 geological reservoir in central Italy. International Journal of Greenhouse Gas Control 12, 72–83. 10.1016/j.ijggc.2012.11.010.

Tsujiura, M., 1983. Characteristic frequencies for earthquake families and their tectonic implications: evidence from earthquake swarms in the Kanto District, Japan. Pure Appl. Geophys. 121, 574-600.

Valoroso, L., Chiaraluce, L., , Piccinini, D., DiStefano, R., Schaff, D., Waldhauser, F., 2013. Radiography of a normal fault system by 64,000 high-precision earthquake locations: The 2009 L'Aquila (central Italy) case study, J. Geophys. Res. Solid Earth 118, 1156–1176, doi:10.1002/jgrb.50130.

Waldhauser, F., 2001. HypoDD: A computer program to compute double-difference earthquake locations, U.S. Geol. Surv. Open File Rep., 01-113.

Waldhauser, F., Ellsworth, W.L., 2000. A double-difference earthquake location algorithm: Method and application to the northern Hayward Fault, California. Bull. Seismol. Soc. Am., 90, 1353–1368.

Wernicke, B., 1995. Low-angle normal faults and seismicity: A review. J. Geophys. Res. 100, 20,159–20.

Wiemer, S., Wyss, M., 2000. Minimum magnitude of complete reporting in earthquake catalogs: Examples from Alaska, the Western United States, and Japan. Bull. Seismol. Soc. Am. 90, 859–869.

Zhinzhin M.N., Gvishiani, A.D., Rouland, D., Bonnin, J., Mohammadioun, B., 1994. Identification of geological region for earthquakes using syntactic pattern recognition of seismograms. Natural Hazards 10, 139-147.

Zhinzhin, M.N., Gvishiani, A.D., Bottard, S., Mohammadioun, B., Bonnin, J., 1992. Classification of strong motion waveform from different geological regions using syntactic pattern recognition scheme. Cahiers du centre Européen de Géodynamique et de Séismologie, Luxembourg, Grand-Duché de Luxembourg 6, 33-42.

Web references

Locati, M., Camassi, R., Stucchi, M., 2011. DBMI11, the 2011 version of the Italian Macroseismic Database. Milano, Bologna, http://emidius.mi.ingv.it/DBMI11 Accessed 20 December 2012.

Monachesi, G., Marzorati, S., Ladina, C., Cattaneo, M., Frapiccini, M., D'Alema, E., Carannante, S., 2012. Beach Balls in central western Italy. The focal mechanisms of the Earthquakes recorded by the RESIICO (central oriental Italy seimological network). Istituto Nazionale di Geofisica e Vulcanologia. http://www.an.ingv.it/BB/home.html Accessed 20 December 2012.

USGS, CERI, ISTI and the Earthworm Community 2010. Earthworm Documentation V7.4. http://folkworm.ceri.memphis.edu/ew-doc/ Accessed 20 December 2012.

Tab.1 Focal mechanisms of the ML ≥2 seismic events with more than 20 polarities. IDFM, identifier of the focal mechanism. Data base: source of the parameters. BB, Beach Balls data base (Monachesi et al., 2012). DTMT, Time Domain Moment Tensor data base (Scognamiglio et al., 2009). Present: the present study is the source. ML, local magnitude. Mw, moment magnitude. Strike, strike direction of the mechanism. Dip, angle of dip of the mechanism. Rake, angle of the rake of the mechanism. Family ID, identifier of the family detected by the waveforms of the PIEI station with a cross-correlation threshold of 0.90.

Figure captions

Fig.1. The seismicity, seismic network, and tectonic framework of the Umbria-Marche region. Black circles; seismicity from August 2009 to January 2012. Red circles; seismicity from April 10-30, 2010. Yellow star, the April 15, 2010 (01:47), M_L 3.8 earthquake. Black squares, historical earthquakes. White stars, recent moderate earthquakes. Light blue triangles, INGV seismic

stations. Red triangles, seismic stations used to relocate the seismic sequence of the April 2010. Inset: Umbria-Marche region in relation to Italy.

Fig.2. Seismic events of the Pietralunga area from August 1, 2009 to January 31, 2012. The different colors of the circles indicate the time intervals before, during and after the seismic sequence. Black lines, depth (km) of the ATF fault plane from geological data.

Fig.3. Increase in seismicity rates. Cumulative number of seismic events in the Pietralunga area from August 1, 2009 to January 31, 2012. Yellow curve, 53 events from August 1, 2009 up April 9, 2010 (before the sequence). Red curve, 1283 events from April 10 to April 30, 2010 (sequence). Blue curve, 927 events from May 1, 2010, to January 31, 2012 (after the sequence).

Fig.4. Number of seismic events per day in the Pietralunga area. a) From August 1, 2009 to April 9, 2010. b) From April 10 to April 30, 2010. c) From May 1, 2010 to January 31, 2012.

Fig.5. Magnitude distribution of the Pietralunga sequence. a) Magnitude of the seismic events from April 10 to April 30, 2010; b) Magnitude histogram; c) Inset: percentage of seismic events for each magnitude range.

Fig.6. Pattern of the Pietralunga sequence. a) Pietralunga sequence before the relocation; b) Pietralunga sequence after the relocation. Gray circle, absolute location of the seismicity recorded from August 2009 to January 2012. Blue circles, absolute locations of the seismic events selected for relocation. red circles, relative locations of cluster 1. Magenta circles, relative locations of cluster 2. Yellow star, M_L 3.8 April 15, 2010 earthquake before (a) and after (b) the relocation process. Red Triangle, seismic stations for relocation. A-A' black line, profile of the section of the Fig. 7.

Fig.7. Vertical section 217° N of the Pietralunga sequence relocated seismic events. Red circles, hypocenters of cluster 1. Magenta circles, hypocenters of cluster 2. Black line, projection of an angle of 65° from the surface.

Fig.8. Parameters of the relocations. a) Histogram of the azimuthal gap of the relocations. b) percentage of the relocatons with at leat a certain number of phases. c) Overlap of the relocated hypocenters obtained with increasing squared cross-correlation values (cc), moving from 0.49 (red symbols, cc of 0.70) to 0.90 (light blue symbols, cc of 0.95). NO, all of the events with any cross-correlation threshold. Black line B-B', profile of the section in panel d; d) Section along B-B' line.

Fig.9. Horizontal time-space evolution of the seismic migration from 5 days before to 35 days after the mainshock. Coordinates (0,0): space-time position of the mainshock. Positive distances, NW direction along 307° N. Coulored circles, seismic events belonging to a family (see family ID family). Gray circles, seismic events not belonging to any family. Yellow-red star, M_L 3.8 April 15, 2010, seismic event. Yellow-black stars, $M_L \geq 2$ seismic events. a-b) Space-time interval of the uninterrupted migration. A, C1, C2, E, F) intervals of the gradual migration. B, D: intervals of the abrupt migration.

Fig.10. Vertical time-space evolution of the seismic migration from 5 days before to 35 days after the mainshock. Colored symbols, seismic events belonging to a family (see family ID in the legend). Gray circles, seismic events not belonging to any family. Yellow-red star: M_L 3.8 April 15, 2010, seismic event. Yellow-black stars, $M_L \geq 2$ seismic events.

Fig.11. Map of the Pietralunga seismic sequence migration. D = 0: origin time of the mainshock (April 15, 2010, 01:45:37 UTC). 1 D = 24 h. a) Seismic events from 5 to 2 days before the mainshock. b) Seismic events from 2 days before mainshock to the mainshock. c) Seismic events from the mainshock to 24 h after the mainshock. d) Seismic events from 24 to 48 h after the mainshock. e) Seismic events from 48 to 72 h after the mainshock. g) Seismic events from 4 to 12

days after the mainshock. h) Seismic events of the on day 12 after the mainshock. Beach balls, focal mechanisms of the events listed in Tab. 1. Gray circles, relocated events of the Pietralunga sequence. Colored symbols, seismic events belonging to a family (see family ID in the legend of Fig.9). Black circles, seismic events not belonging to any family. Yellow-red star, M_L 3.8 April 15, 2010, seismic event. Yellow stars, $M_L \geq 2$ seismic events not belonging to a family. Black stars, $M_L \geq 2$ seismic events not belonging to any family. Beach balls, focal mechanisms calculated for the events with $M_L \geq 2$.

Panels (a) and (b) show the location of the seismicity before the main event. In panel (c), the increase in seismicity, is appreciable and occurred just after the main event. From panel (d) to (h), the frames show the clear migration towards the NW that occurs through the seismicity pattern with a non uniform shape.

Fig.12. Example of the splitting of a family by an increase of the cross-correlation threshold. CC, normalized cross-correlation coefficient. a) Map of the families identified by the PIEI station signals. Gray circles, relocated events of the Pietralunga sequence. Black circles, threshold 0.90, Family 2. Blue circles, threshold 0.95, Family 14. Red circles, threshold 0.95, Family 25. b) PIEI station waveforms of the 126 seismic events that belong to family 2 at threshold 0.90. c) Some events belonging to family 2 at threshold 0.90. Blue curves, threshold 0.95, Family 14. Red curves, threshold 0.95, Family 25.

Fig.13. Vertical map (section 307°N) of the cumulative seismicity of the Pietralunga sequence migration. The frames describe the time evolution of the seismicity, showing the events that occurred in following time step (each one overlapping the other). Each panel shows a longitudinal section of the structure while each square of the grid represents 1 km^2 on the vertical plane. D = 0, origin time of the mainshock (April 15, 2010, 01:45:37 UTC). D unit = 24 h. Gray circles, relocated events of the Pietralunga sequence. Colored symbols, seismic events belonging to a family (see family ID in the legend of Fig. 9). Black circles, seismic events not belonging to any family. Yellow-red star, M_L 3.8 April 15, 2010, seismic event. Yellow stars, ML ≥2 seismic events not belonging to

a family. Black stars: M_L ≥2 seismic events not belonging to any family. Panels: a) Seismic events from 5 days before the mainshock to 2 days before the mainshock. b) Seismic events up to the mainshock. Multiplets 6 and 7 arise from the next mainshock area c) Seismic events up to 24 h after the mainshock. The seismicity spans in a NW and SE direction. Only the events belonging to family 3 are characterized by a depth >5 km. Families 10 and 12 arise near the main hypocenter, whereas families 2 and 3 start beyond the NW edge of families 12 and 10, respectively. d and e) In the next 2 days, the deepening of the migration involved many events for family 3. Family 2 did not migrate but family 25 appears in front of its, with few events localized at a depth of 4.5 km. f) In 24 hours, three days after the main event, the migration of family 3 fills 1 km^2 (in few hours) at a depth of 5 to 6 km, with a high rate of micro-seismicity added to 11 events with M_L ≥2. Few events belonging to family 25 (the upper portion of the sequence) occurred on this day; the migration at a depth ranging between 4 and 5 Km appears locked with respect to the lower migration represented by family 3. g) Seismic events up to 12 days after the mainshock. The seismicity remains the same, as shown in the previous panels; only a few events that belong to family 35 occur near to and above family 25. The seismicity on a distinct structure and highlighted by 19 family evolves. h) Seismic events up to 13 days after the mainshock. The end of the migration happens in the deepest portion of the structure only, on a patch with dimension lesser than 1 km^2. The propagation of seismicity is still locked between 4 km and 5 km in depth.

Fig.14 a) Map of the ATF isobaths (black thin lines, depth in km) and the positions of the S1 (c) and S3 (d) sections with respect to the Pietralunga seismic sequence epicenters (black points). b) Structural features and CO_2 geological storage in the Triassic Evaporites (modified from Trippetta et al., 2013). c) Geological sketch of S1 section. d) Geological sketch of the S3 section. S1 and S3 are simplified and modified from Mirabella et al. (2011). The sedimentary column that lies in the hanging wall of the ATF is composed of layers of turbidites and Marls, Oligocene-Miocene (TM), carbonates, Jurassic-Eocene(C) and evaporites, Triassic (E). Layer E is represented by an about 2 km thick, low Vp horizon composed of clastic and methamorphic rock, located above the crystalline basement (Mirabella et al., 2008). The contact between the Evaporites and the top of the

basement shows an inversion of Vp from more than 6.0 km/s (Bally et al., 1986; Barchi et al., 1998a) to less than 5.0 km/s (Mirabella et al., 2008).

Fig.A.1. Cross-correlation matrix at the PIEI station. Gray scale: normalized cross-correlation coefficient.

Fig.A.2. Histogram of normalized cross-correlation coefficients of the PIEI cross-correlation matrix. The dotted line indicates the limit where the distribution deviates from a pure normal distribution.

Fig.A.3. Number of families and components of each family at the different cross-correlation coefficient thresholds. CC: normalized cross-correlation coefficient.

Table 1

Click here to download Table: Table_1.docx

IDMF	Data Base	M_L	Strike(°)	Dip(°)	Rake(°)	Family ID
M01	Present	2.1	300	60	-90	6
M02	Present	2.0	300	50	-90	X
M03	BB	3.8	355	60	-90	X
M03	DTMT	3.8 (Mw)	307	61	-99	X
M04	BB	2.8	325	80	-92	X
M06	BB	2.4	300	55	-90	2
M07	BB	2.7	329	71	-97	2
M10	BB	2.0	320	55	-90	2
M11	BB	2.5	297	62	-101	X
M12	BB	2.9	272	61	-84	3
M12	DTMT	2.83 (Mw)	302	72	-95	3
M13	BB	2.7	329	70	-94	X
M16	BB	2.2	295	55	-90	3
M19	BB	2.2	295	55	-90	3
M20	BB	2.3	300	60	-90	3
M22	BB	2.5	320	60	-90	X
M25	BB	2.1	303	56	-97	3
M26	BB	2.1	300	55	-90	37
M28	BB	2.2	300	55	-90	37
M30	Present	2.1	163	51	-82	19

TABLE 1

Figure 1

Click here to download high resolution image

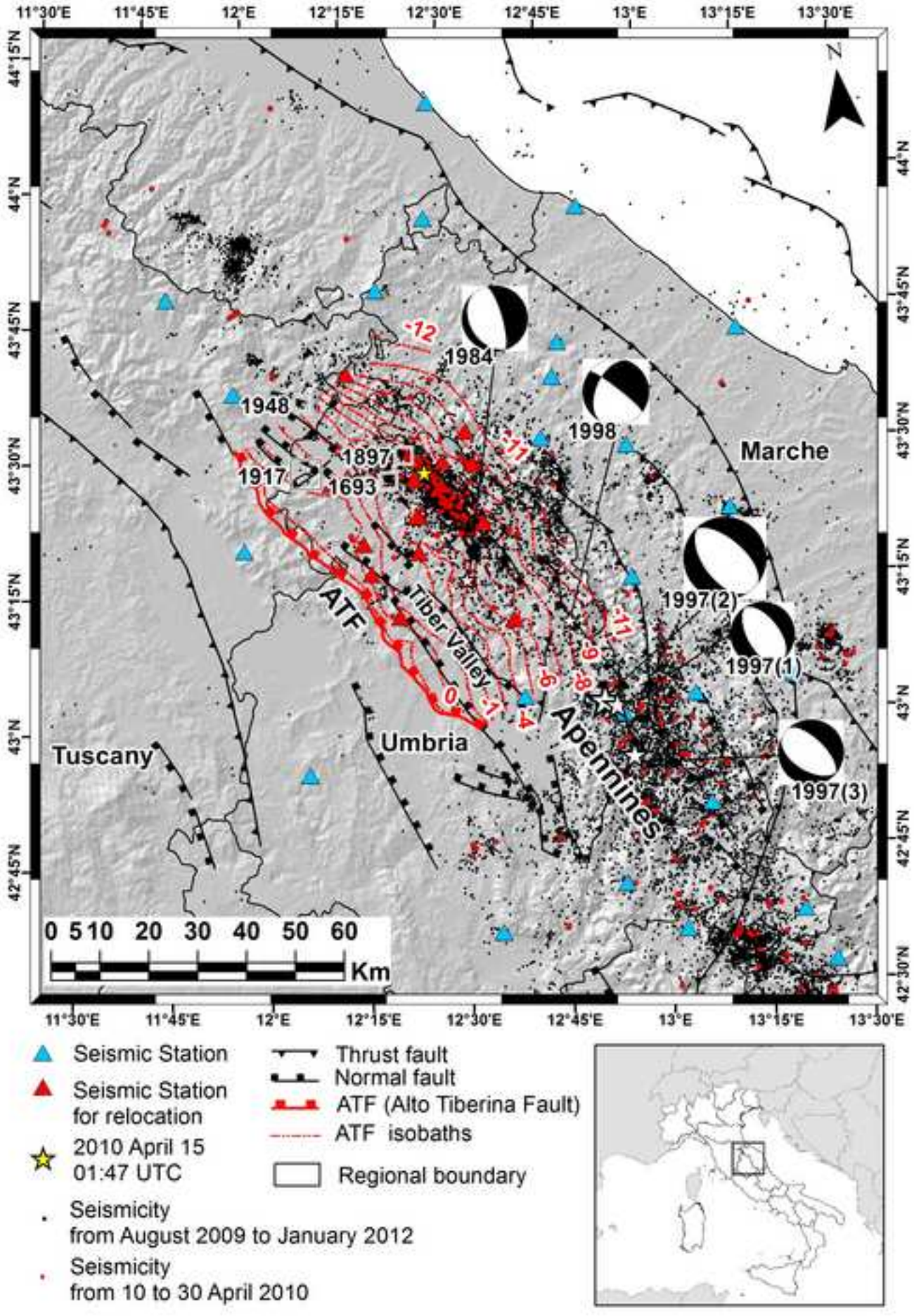

Figure 2

Click here to download high resolution image

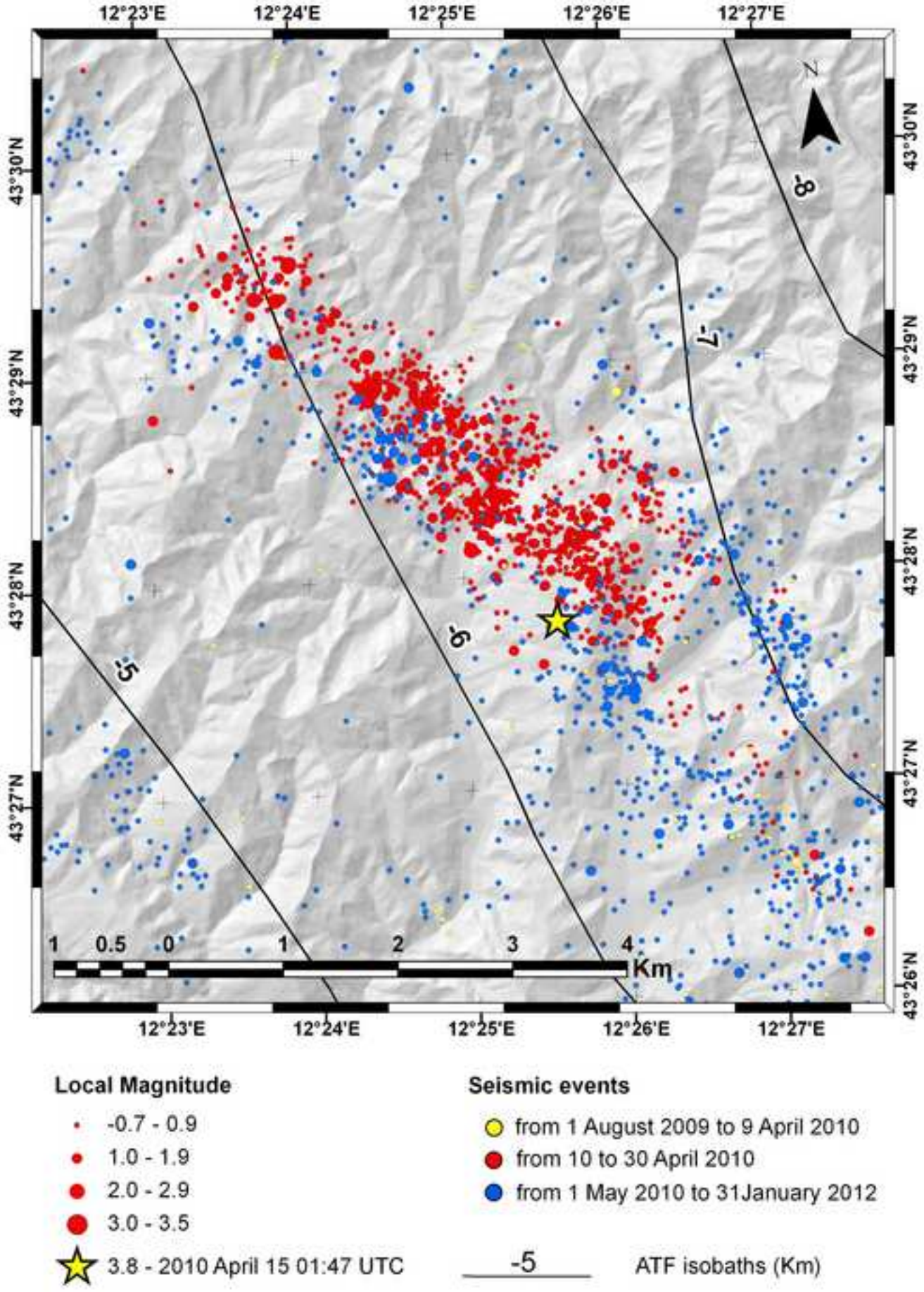

Figure 3

Click here to download high resolution image

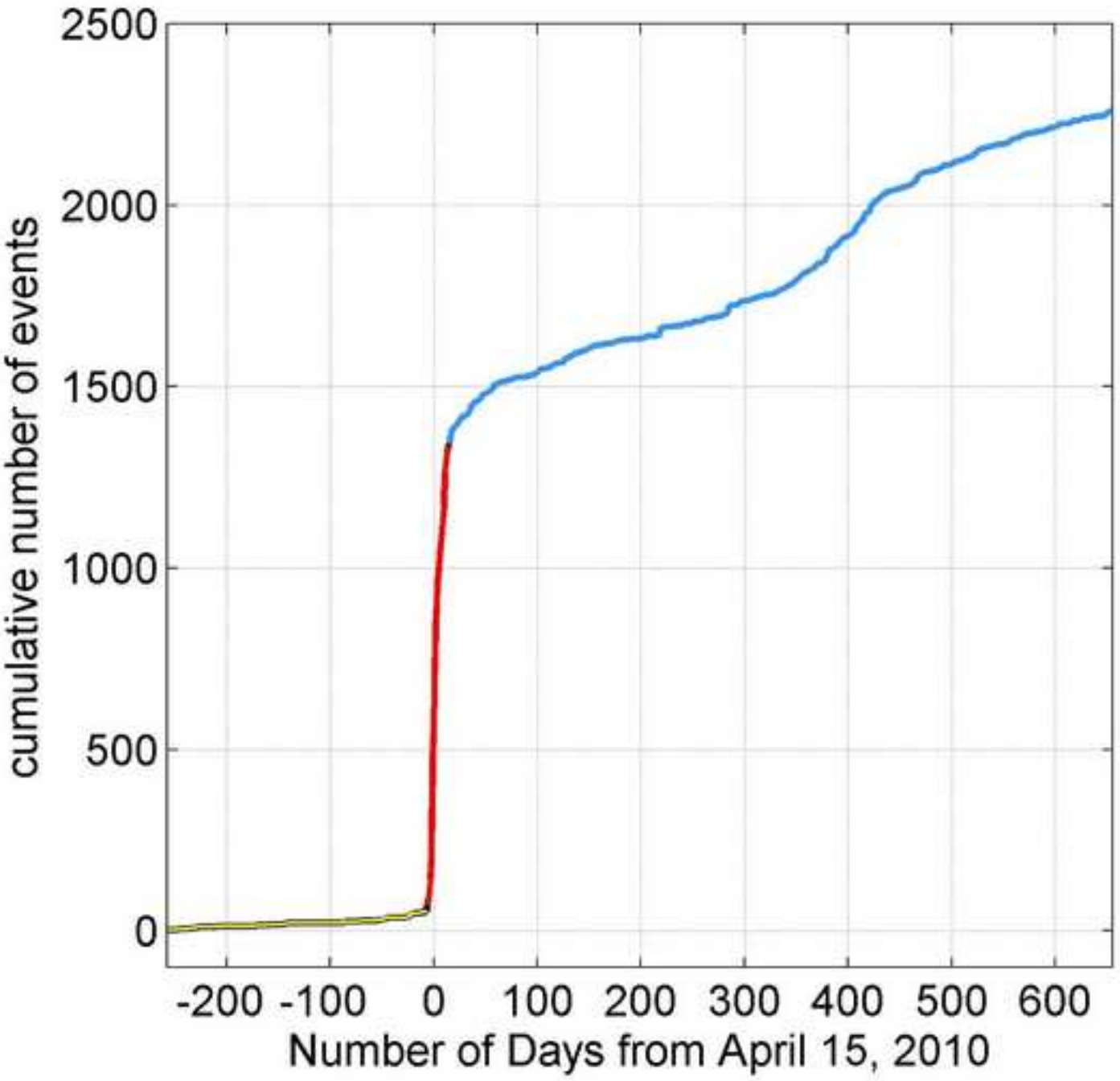

Figure 4

Click here to download high resolution image

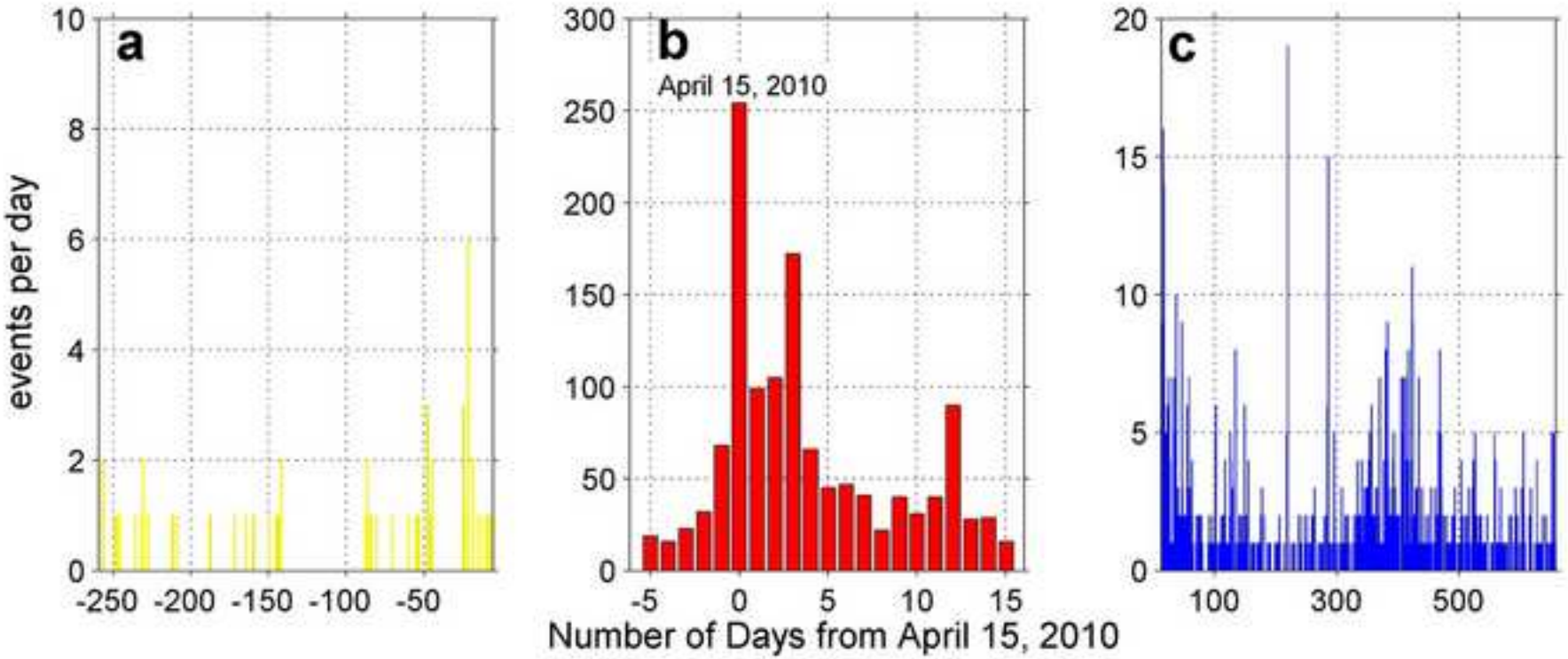

Figure 5

Click here to download high resolution image

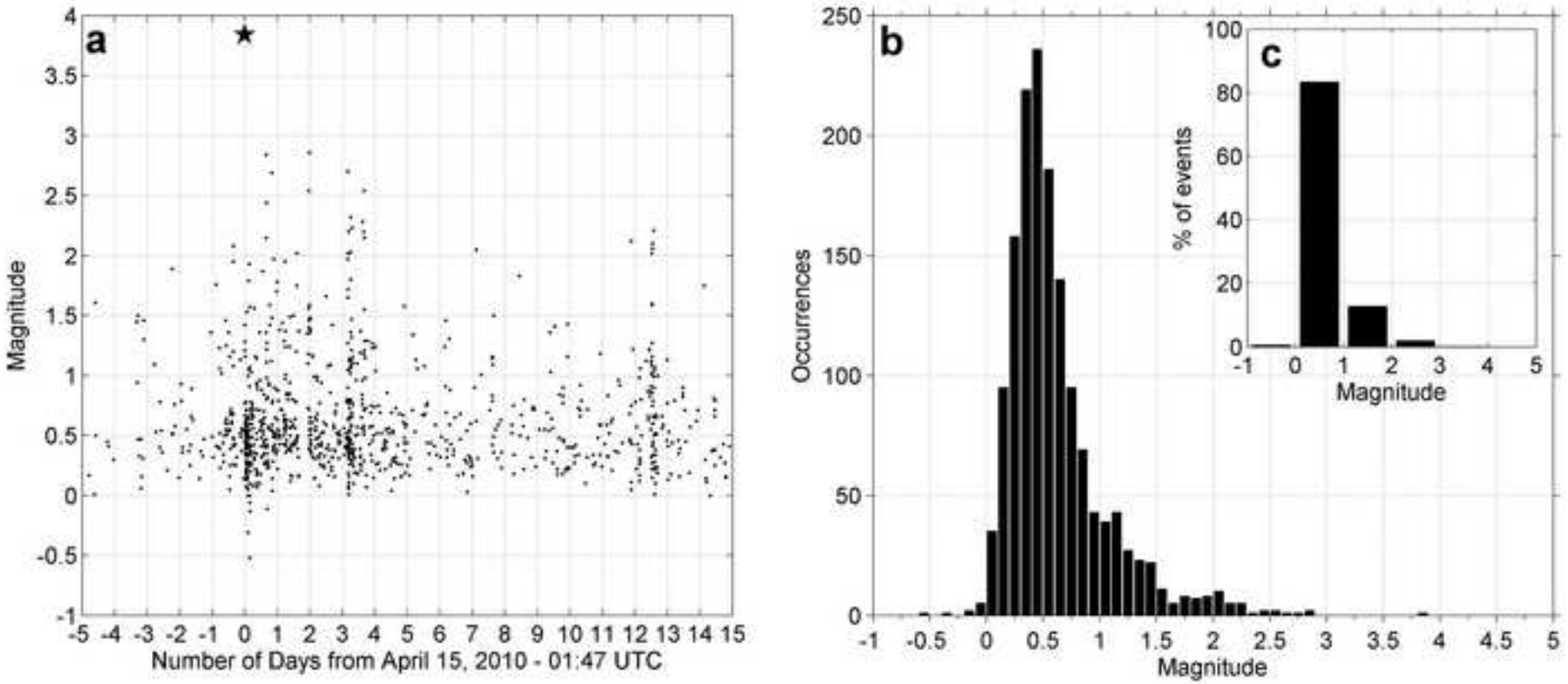

Figure 6

Click here to download high resolution image

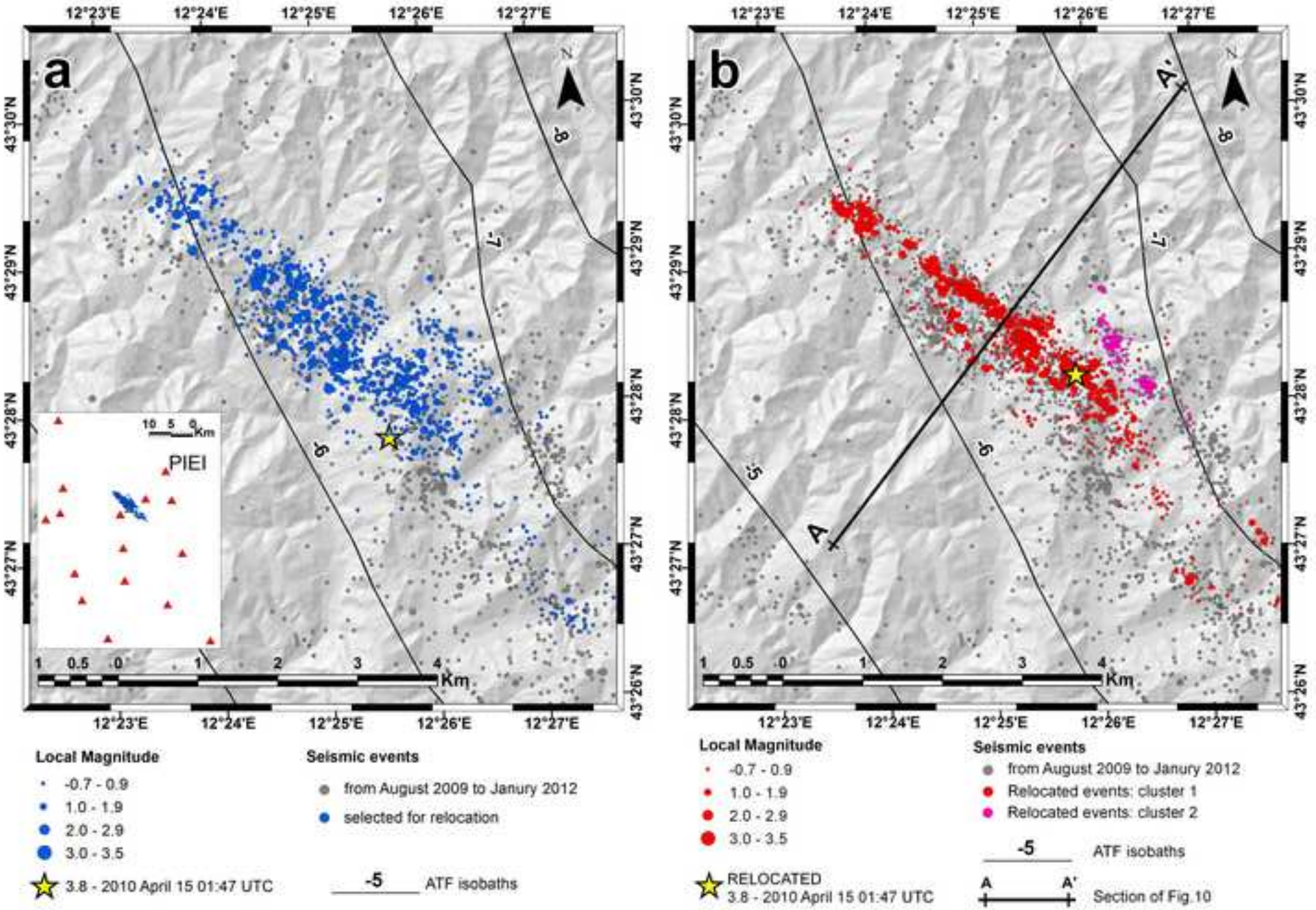

Figure 7

Click here to download high resolution image

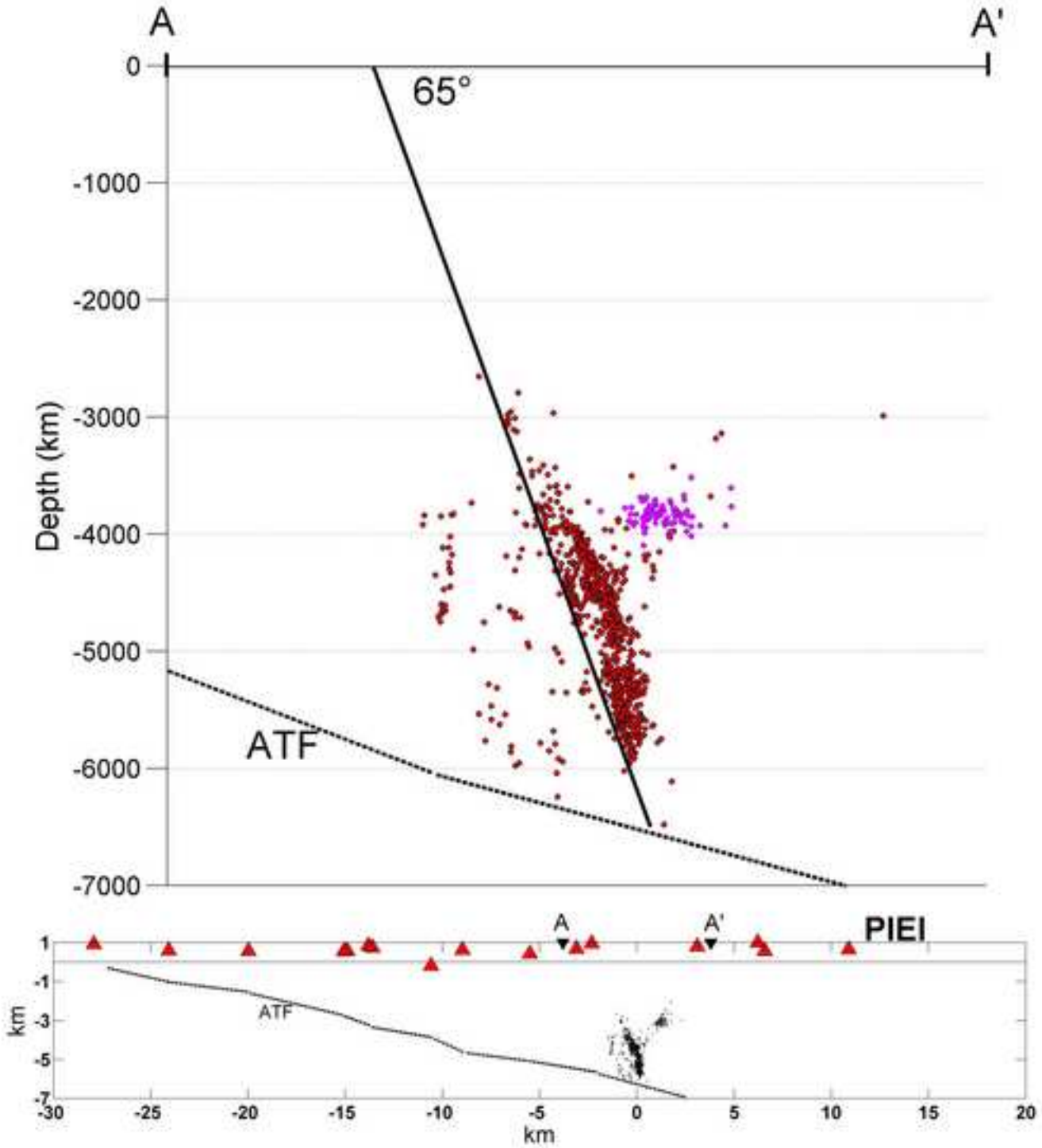

Figure 8

Click here to download high resolution image

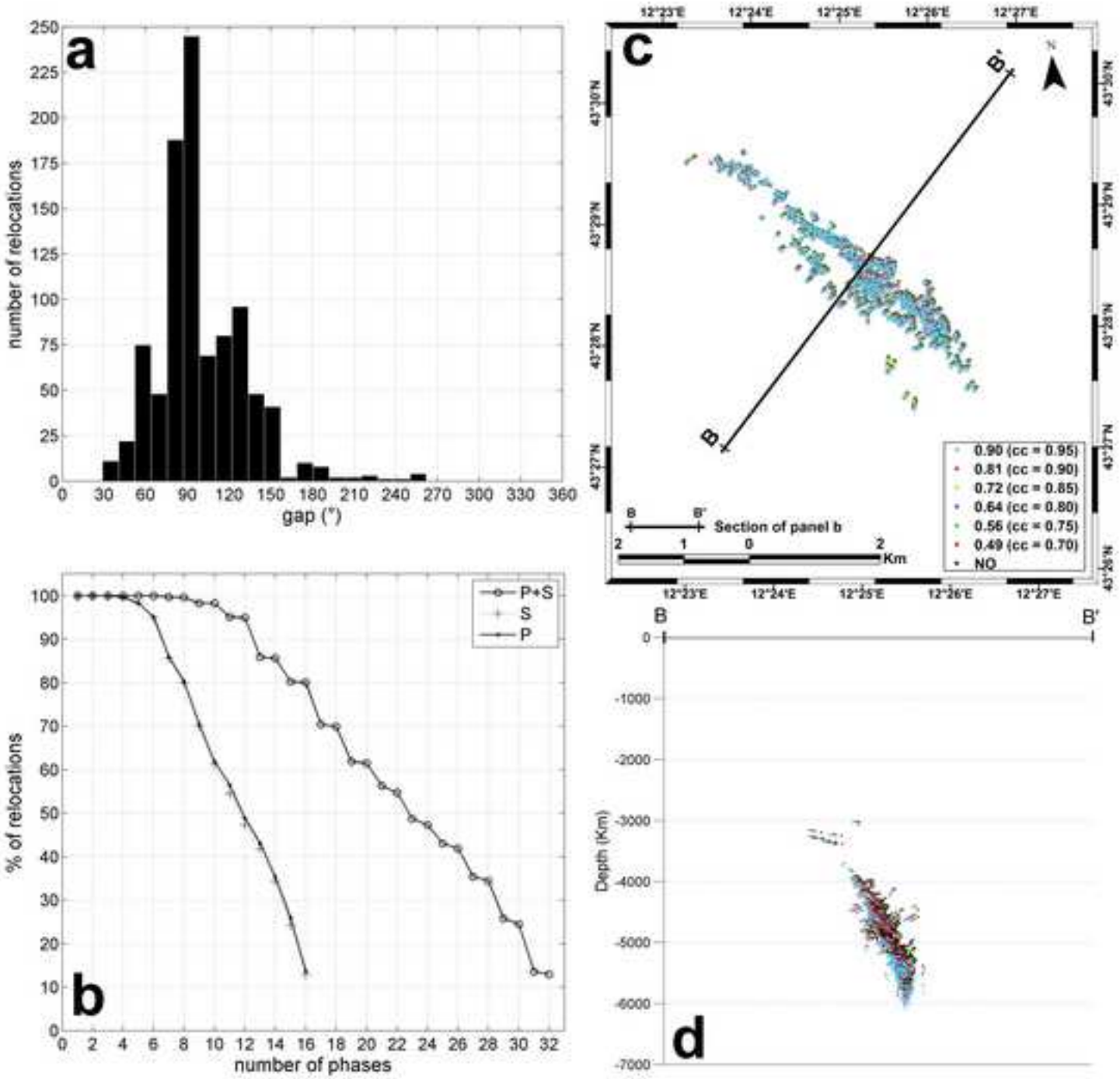

Figure 9

Click here to download high resolution image

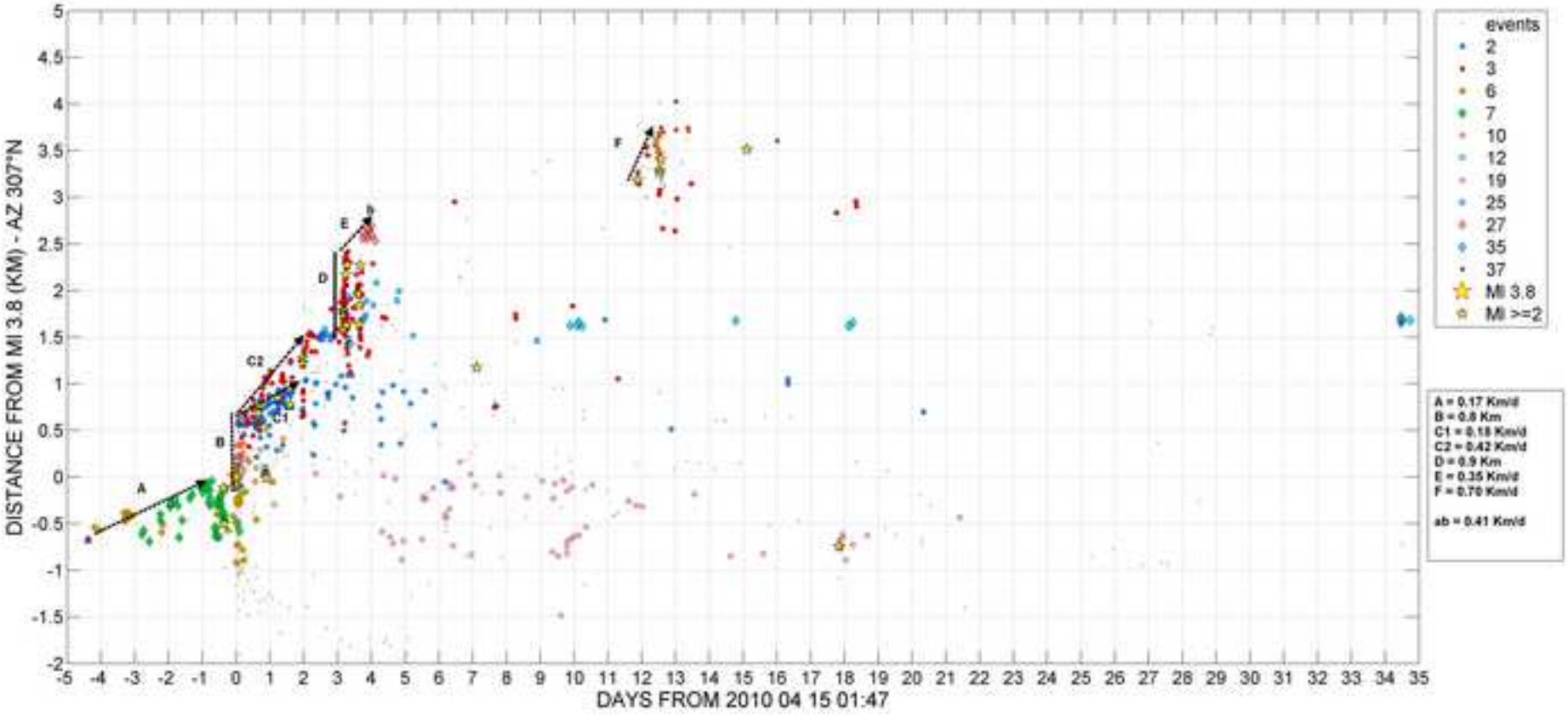

Figure 10

Click here to download high resolution image

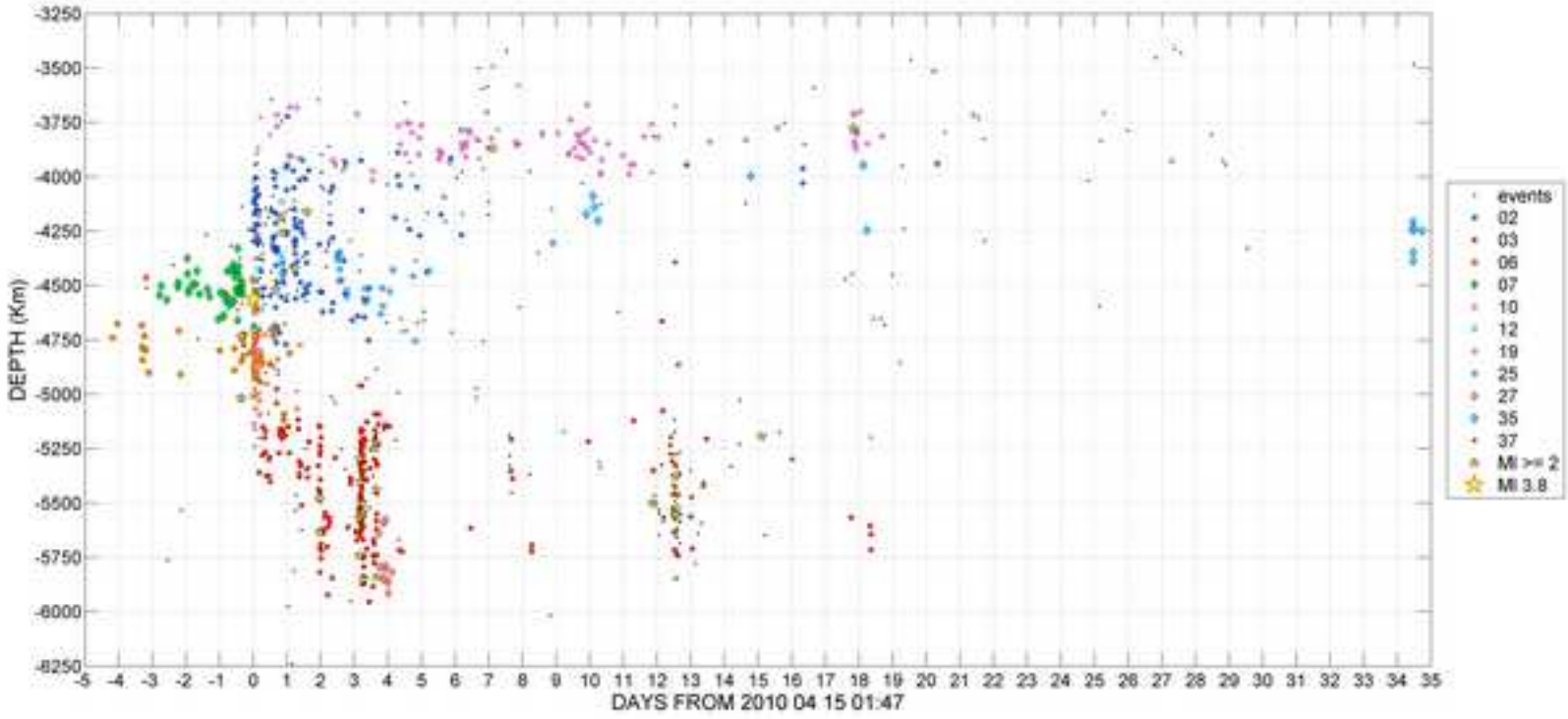

Figure 11

Click here to download high resolution image

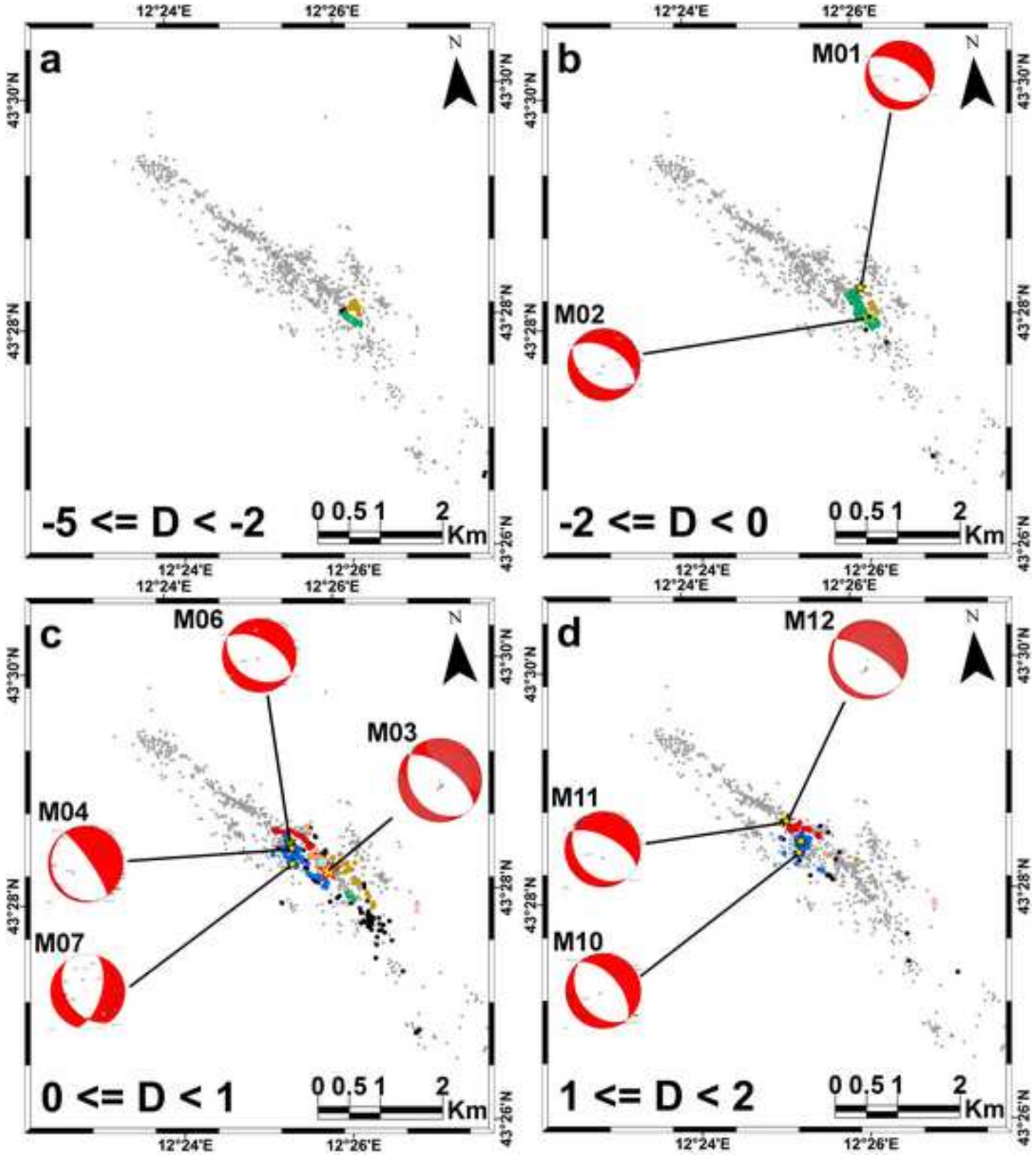

Figure 11 continue

Click here to download high resolution image

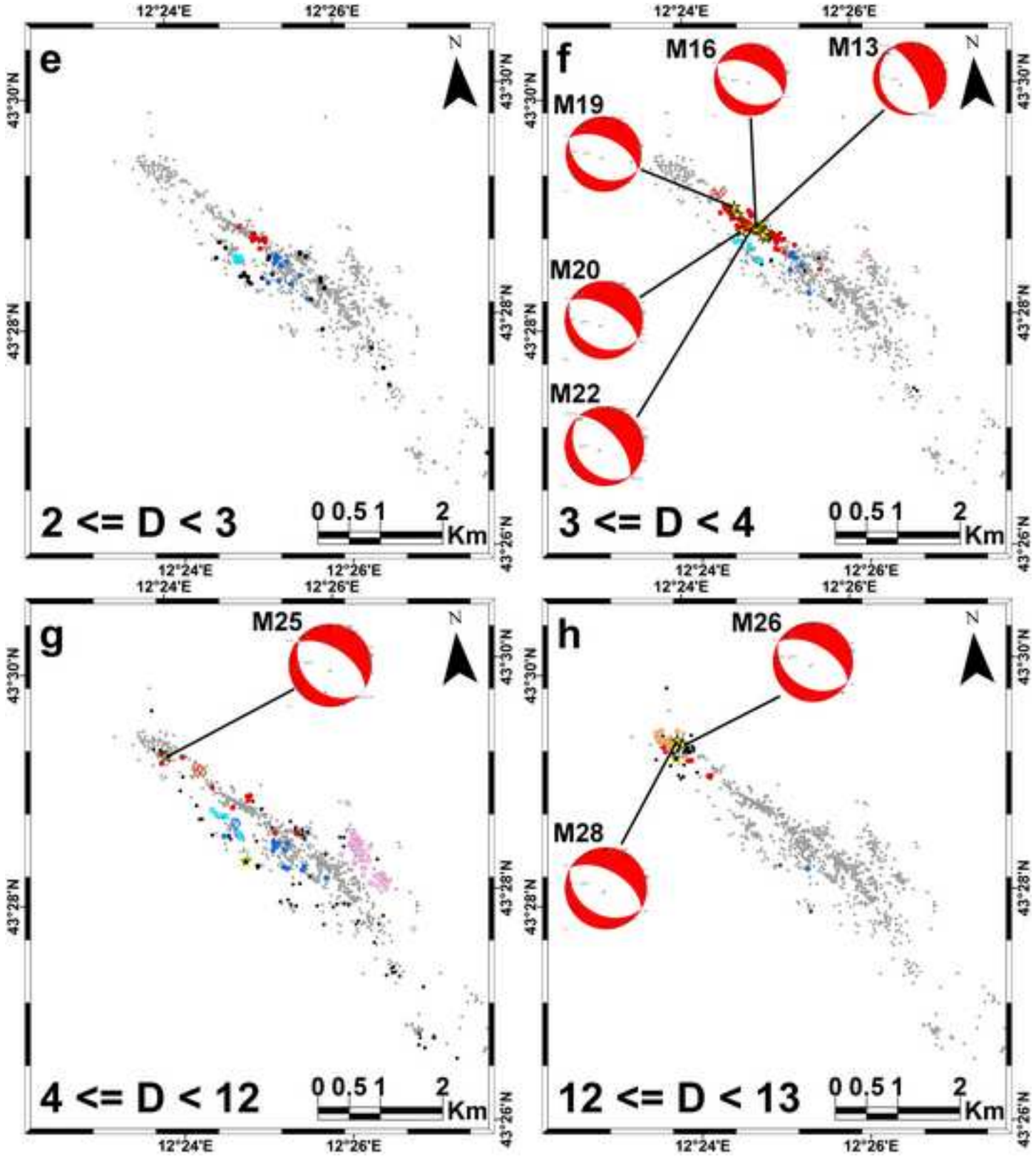

Figure 12

Click here to download high resolution image

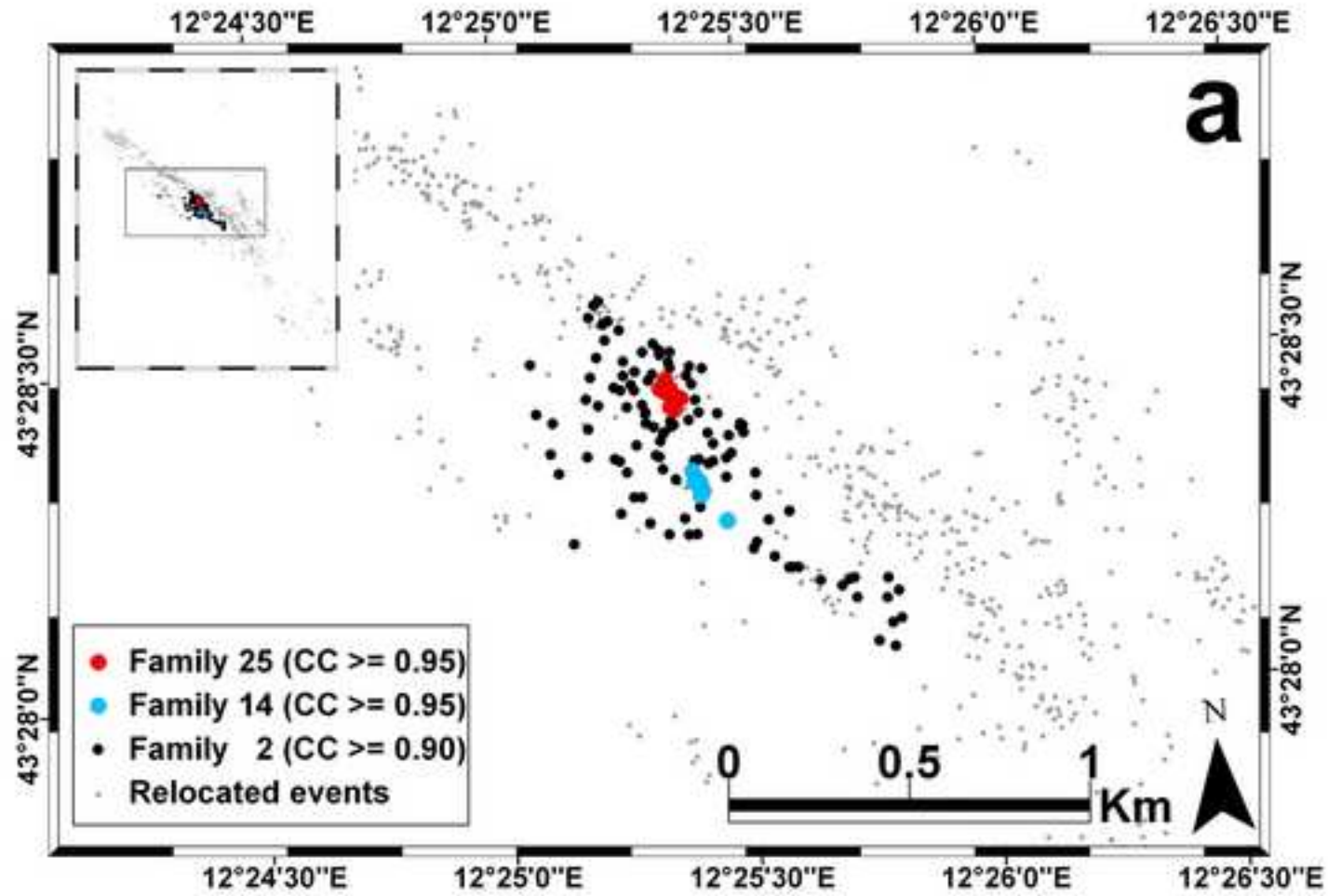

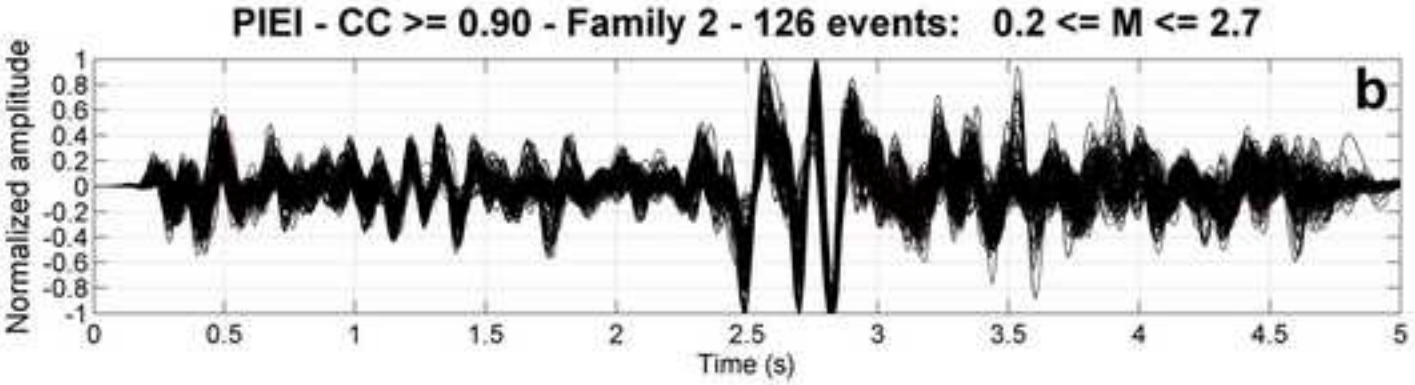

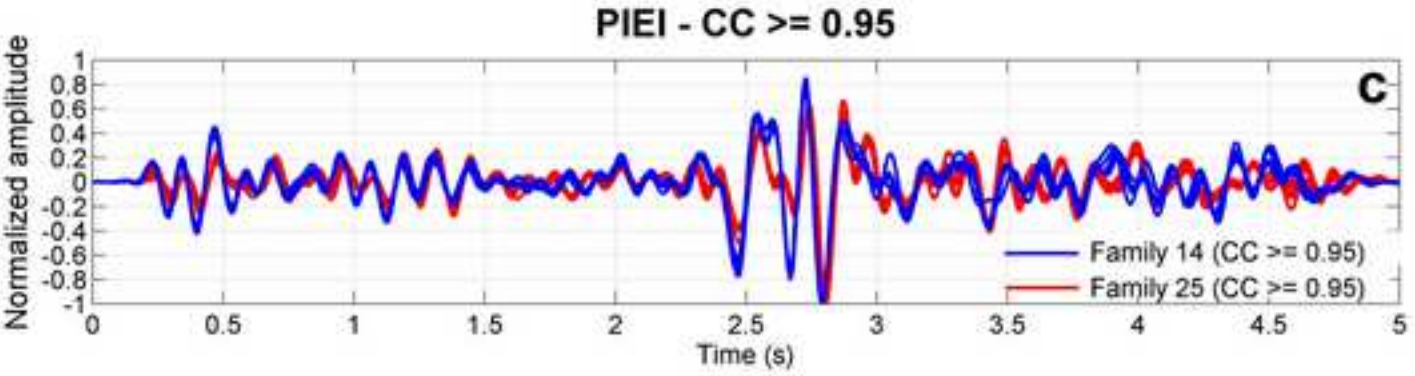

Figure 13

Click here to download high resolution image

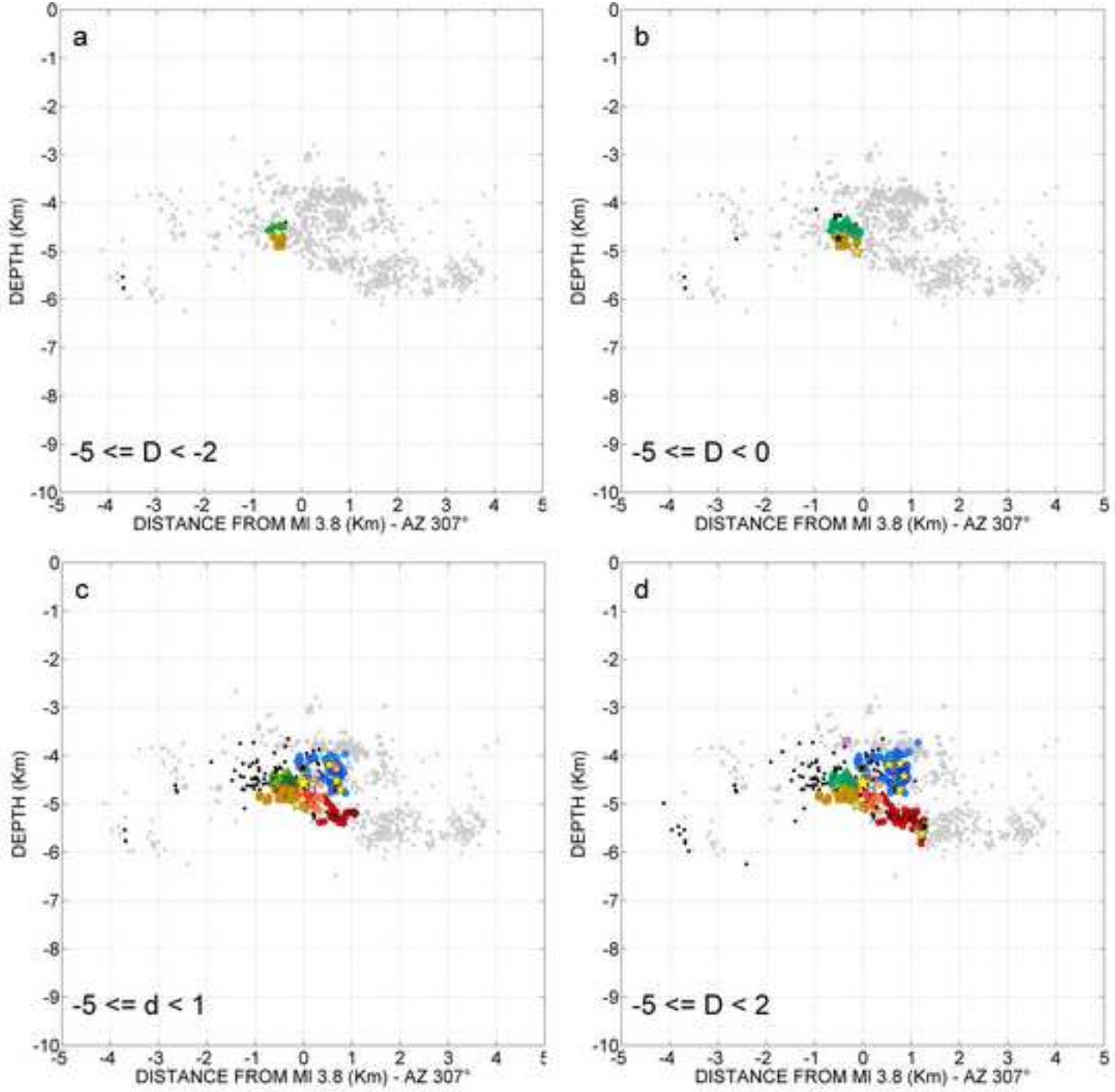

Figure 13 continue

Click here to download high resolution image

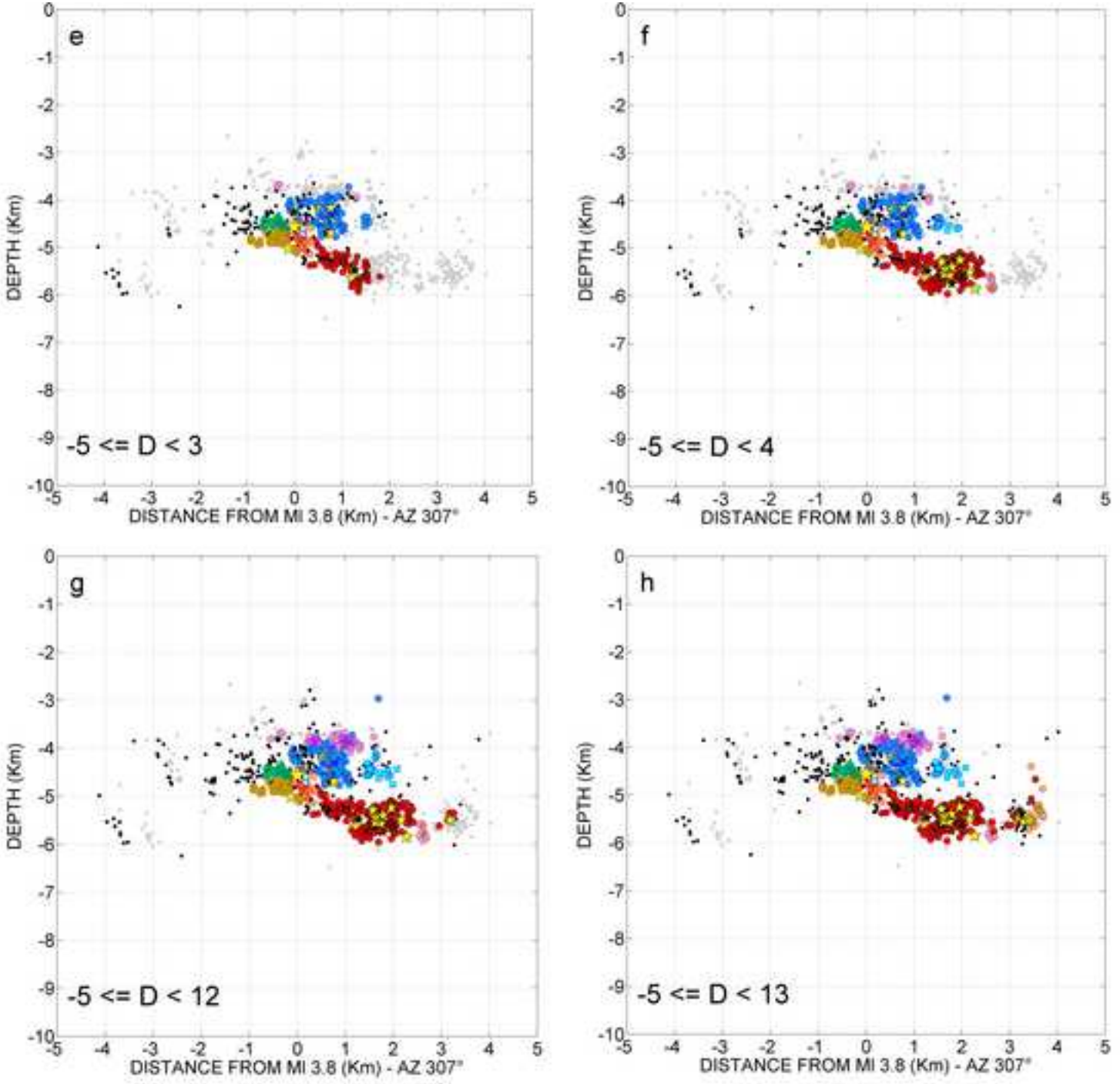

Figure 14

Click here to download high resolution image

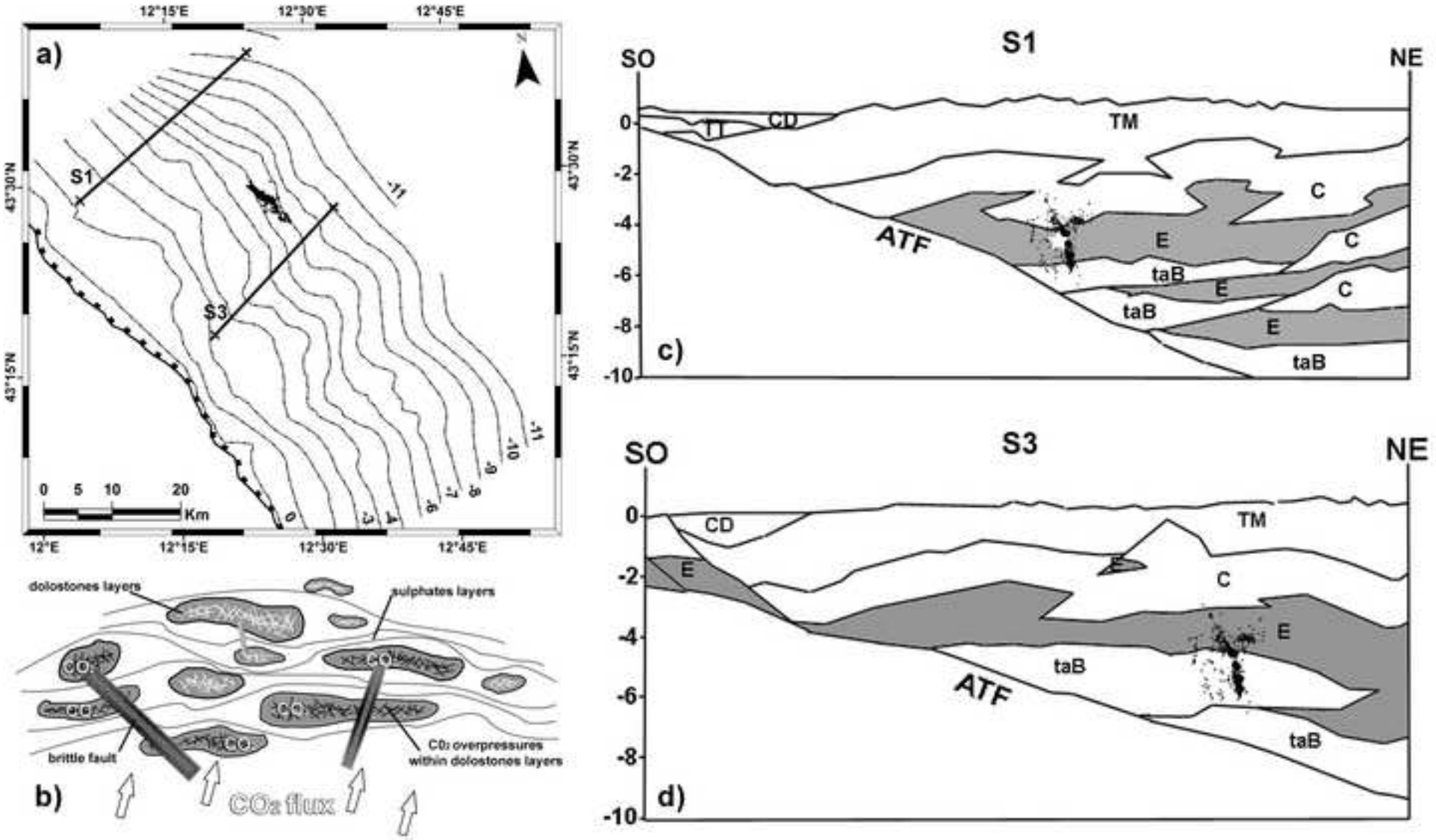

Figure A1

Click here to download high resolution image

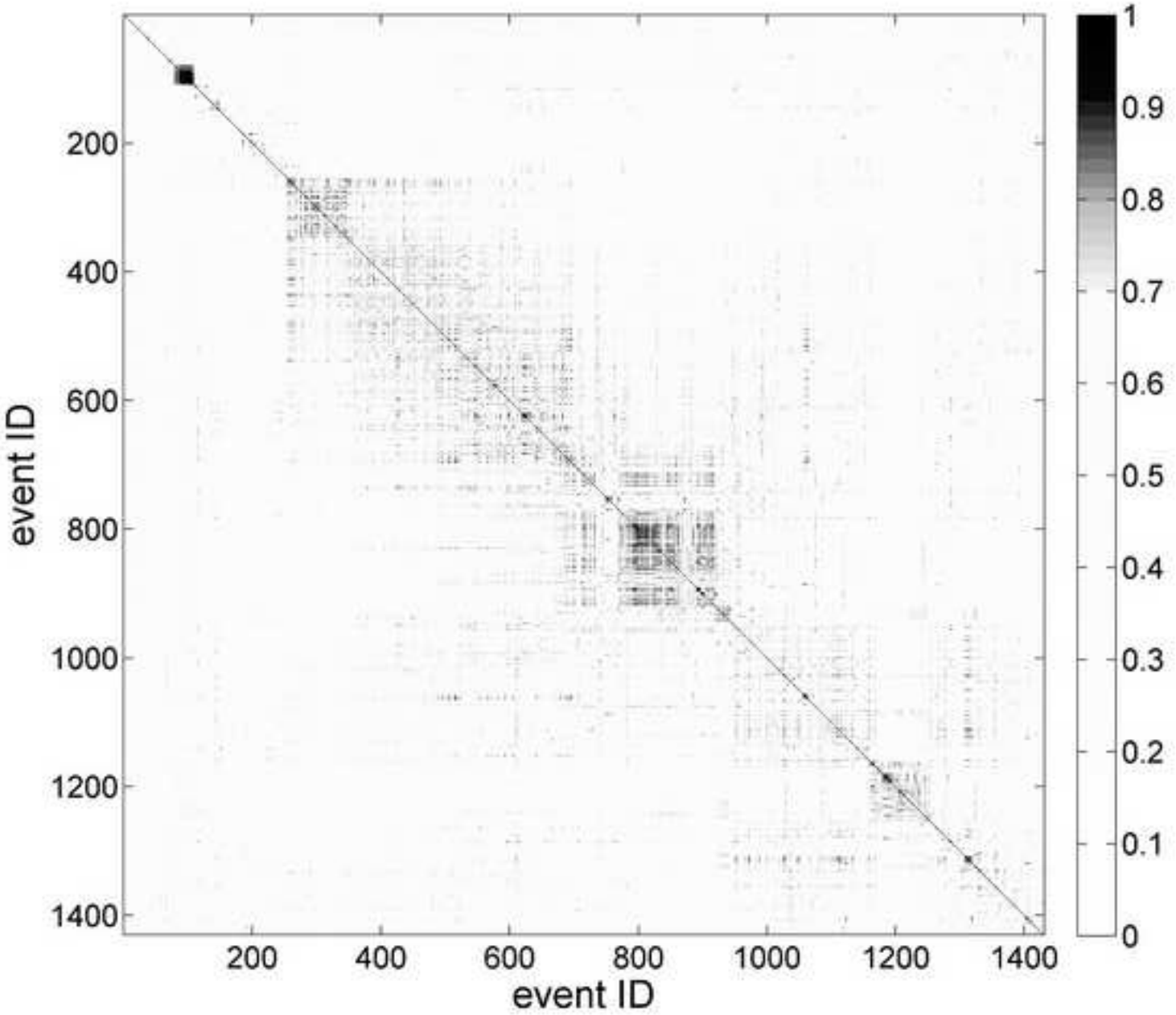

Figure A2

Click here to download high resolution image

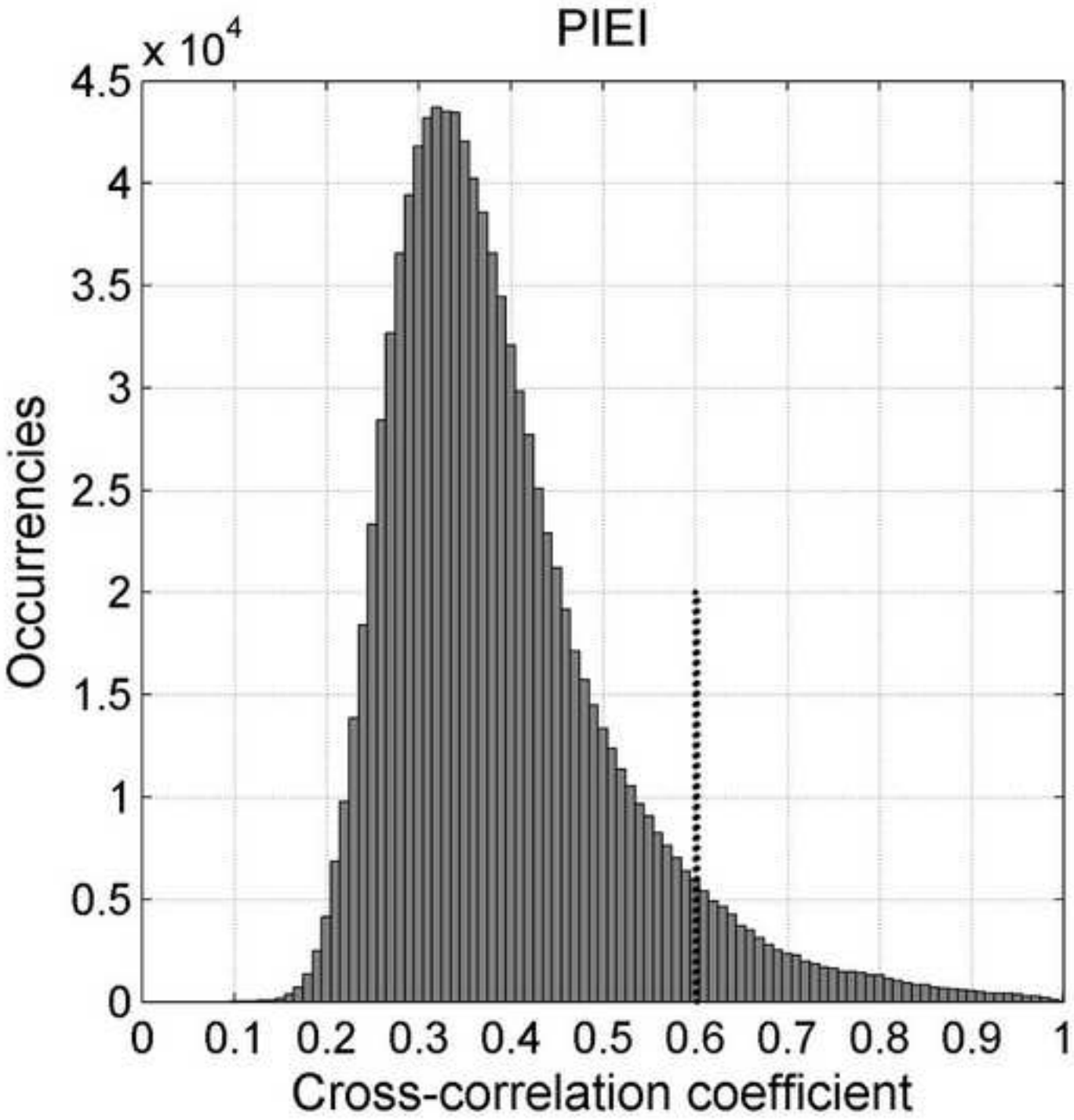

Figure A3

Click here to download high resolution image